OPTIMIZATION OF A HEAT SINK WITH HETEROGENEOUS HEAT FLUX BOUNDARY CONDITION

A THESIS SUBMITTED TO
THE GRADUATE SCHOOL OF NATURAL AND APPLIED SCIENCES
OF
MIDDLE EAST TECHNICAL UNIVERSITY

BY

EREN TURGUT

IN PARTIAL FULFILLMENT OF THE REQUIREMENTS
FOR
THE DEGREE OF MASTER OF SCIENCE
IN
MECHANICAL ENGINEERING

DECEMBER 2019

Approval of the thesis:

OPTIMIZATION OF A HEAT SINK WITH HETEROGENEOUS HEAT FLUX BOUNDARY CONDITION

submitted by **EREN TURGUT** in partial fulfillment of the requirements for the degree of **Master of Science in Mechanical Engineering Department, Middle East Technical University** by,

Prof. Dr. Halil Kalıpçılar
Dean, Graduate School of **Natural and Applied Sciences** _____

Prof. Dr. M. A. Sahir Arıkan
Head of Department, **Mechanical Engineering** _____

Prof. Dr. Almıla Güvenç Yazıcıoğlu
Supervisor, **Mechanical Engineering, METU** _____

Examining Committee Members:

Assoc. Prof. Dr. Cüneyt Sert
Mechanical Engineering Dept., METU _____

Prof. Dr. Almıla Güvenç Yazıcıoğlu
Mechanical Engineering, METU _____

Prof. Dr. Tuba Okutucu Özyurt
Mechanical Engineering Dept., METU _____

Assoc. Prof. Dr. Nilay Sezer Uzol
Aerospace Engineering Dept., METU _____

Assoc. Prof. Dr. Oğuz Turgut
Mechanical Engineering Dept., Gazi Uni. _____

Date: 03.12.2019

I hereby declare that all information in this document has been obtained and presented in accordance with academic rules and ethical conduct. I also declare that, as required by these rules and conduct, I have fully cited and referenced all material and results that are not original to this work.

Name, Surname: Eren Turgut

Signature:

ABSTRACT

OPTIMIZATION OF A HEAT SINK WITH HETEROGENEOUS HEAT FLUX BOUNDARY CONDITION

Turgut, Eren
Master of Science, Mechanical Engineering
Supervisor: Prof. Dr. Almıla Güvenç Yazıcıoğlu

December 2019, 84 pages

Advancements in micro/nanotechnology along with the size reduction in avionics, raise the importance of microchannel heat sink utilization in the field of electronics cooling. The usage of conventional uniform pin fin arrays or microchannels in the presence of non-uniform heating conditions are not sufficient to overcome the occurrence of the hotspots. Consequently, significant temperature gradients take place at the surface to be cooled. In this study, the effects of some design parameters on the non-uniform pin fin clustering is investigated with numerical and statistical methods. Then, with response surface method, surrogate functions for thermal resistance and pressure drop are obtained as functions of design parameters which are fin diameter, pitch ratio, hotspot fin array length, fin height and fluid mass flow rate. The multi-objective genetic algorithm is preferred for minimization of the thermal resistance and pressure drop which are the objective functions of optimization study. The optimum solution is selected from the best solution set, by employing TOPSIS method (Technique for Order of Preference by Similarity to Ideal Solution). Finally, the selected optimum design is solved numerically and compared with the predicted results

Keywords: Micro pin fin, Heat sink, Hotspot, Laminar flow, Non-uniform clustering

ÖZ

HETEROJEN ISI AKILI SINIR KOŞULLU SOĞUTUCU OPTİMİZASYONU

Turgut, Eren
Yüksek Lisans, Makina Mühendisliği
Tez Danışmanı: Prof. Dr. Almıla Güvenç Yazıcıoğlu

Aralık 2019, 84 sayfa

Mikro/nano teknolojideki gelişmeler ve havacılık elektroniğindeki ekipmanlarda boyut küçülmesi ile birlikte, elektronik soğutma alanında mikro kanallı soğutucu uygulamalarının önemi artmıştır. Düzenli olmayan ısıtma sınır koşulları varlığında, geleneksel düzenli mikro kanal-pin kanatçık kullanımı, sıcak nokta oluşumunun üstesinden gelmekte yetersiz kalmaktadır. Sonuç olarak, soğutulacak yüzeylerde dikkate değer sıcaklık farklılıkları oluşmaktadır. Bu çalışmada, bazı dizayn parametrelerinin düzenli olmayan pin kanatçık kümelenmesine etkileri nümerik ve istatistiksel metodlarla incelenmiştir. Sonrasında, tepki yüzeyi metoduyla, tasarım parametreleri olan kanatçık çapı, adım oranı, sıcak nokta kanatçık sıra uzunluğu, kanatçık yüksekliği ve sıvı debisi cinsinden termal direnç ve basınç düşümünün yerine geçen fonksiyonlar elde edilmiştir. Optimizasyon çalışmasının amaç fonksiyonları olan termal direncin ve basınç düşümünün azaltılmasında çok amaçlı genetik algoritma tercih edilmiştir. En iyi çözüm seti arasından, en uygun sonuç TOPSIS metoduyla seçilmiştir. Son olarak, en uygun seçilen tasarım noktası sayısal olarak çözülmüş ve sonuçlar tahmin edilen sonuçlarla karşılaştırılmıştır.

Anahtar Kelimeler: Mikro pin fin, Soğutucu, Sıcak nokta, Laminar akış, Düzensiz kümelenme

To My Family

ACKNOWLEDGEMENTS

Firstly, I would like to express my thankfulness to Prof. Dr. Almıla Güvenç Yazıcıoğlu for her contributions, guidance, and encouragement throughout my graduate studies. It is an honor to be her student.

Secondly, I am very grateful to my superiors Dr. Mehmet Umut Haliloğlu and Dr. Özkan Altay for their great understanding and tolerance in the company. I am also thankful to my other teammates Kaan Koltuk and Richard Owen since they ease my workload during my thesis studies.

Thirdly, I am very thankful to my colleagues Mehmet Halil Yılmaz and Çağatay Koyuncuoğlu for their assistance and encouragement at the hardest times.

Lastly, I would like to thank my family for their great support, understanding and encourangement.

TABLE OF CONTENTS

APPENDICES

LIST OF TABLES

TABLES

LIST OF FIGURES

FIGURES

LIST OF ABBREVIATIONS

ABBREVIATIONS	
A/C	Aircraft
ACS	Air Cycle System
AHP	Analytic Hierarchy Process
ANOVA	Analysis of Variance
BC	Boundary Condition
CAD	Computer Aided Design
CCD	Central Composite Design
CFD	Computational Fluid Dynamics
CPU	Central Processing Unit
DOE	Design of Experiments
ECS	Environmental Control System
GAA	Goal Attainment Algorithm
HPC	High Performance Computing
LCS	Liquid Cooling System
MOGA	Multi-Objective Genetic Algorithm
NSGA	Non-Dominated Sorting Genetic Algorithm
PAO	Polyalphaolefin
RSM	Response Surface Methodology
SPEA2	Strength Pareto Evolutionary Algorithm
SQP	Sequential Quadratic Programming
T/R	Transmitter/Receiver
TOPSIS	Technique for Order of Preference by Similarity to Ideal Solution
VCCS	Vapor Cycle Cooling System

LIST OF SYMBOLS

SYMBOLS

ρ	Density
μ	Dynamic Viscosity
A_f	Wetted Surface Area
A_p	Fin Cross Section Area
C_p	Specific Heat
d	Fin Diameter
d_{bg}	Background Fin Diameter
d_{hs}	Hotspot Fin Diameter
d_{hyd}	Hydraulic Diameter
H	Heat Sink Height
h	Heat Transfer Coefficient
k_f	Fluid Thermal Conductivity
k_s	Solid Thermal Conductivity
L	Heat Sink Length
L_{hs}	Hotspot Fin Array Length
L_p	Fin Circumference Length
N	Number of Fin
Nu	Nusselt Number
Re	Reynolds Number
S	Longitudinal-Transverse Pitch
V_f	Fluid Volume
W	Heat Sink Width

CHAPTER 1

INTRODUCTION

1.1. General

Modern fighter aircraft (A/C) have various auxiliary systems to fulfill their design objectives. Examples of these systems are environmental control system, fuel system, hydraulic power system, pneumatic power system, life support system, electrical power system, etc. The environmental control system (ECS) is one of the aircraft systems which is responsible for air conditioning, cabin pressurization, smoke removal, defogging, air filtering, avionics cooling, and suppling air for customer systems such as fuel tank pressurization, oxygen system, and anti-g system. In order to provide these tasks, ECS has three main subsystems, which are air cycle system (ACS), liquid cooling system (LCS), and vapor cycle cooling system (VCCS). ACS is responsible for cooling, pressurization and supplying air for customer systems. It receives pressurized air from the compressor of the aircraft engines, which is called 'bleed air' and utilizes bleed air for air conditioning purposes.

On the other hand, VCCS is commonly used as an intermediate medium to extract heat from a heat source to heat sink. For example, it can be used to extract the heat load of cabin to the ambient air. Lastly, liquid cooling system is generally used to cool the avionics equipment. Advanced avionics, radar, and communication systems in fighter aircraft have high heat loads that ACS would not be enough to provide cooling demand with available bleed air because bleed air is precious for aircraft performance and is limited. However, liquid cooling has higher heat transfer rates than air cooling. Moreover, higher density liquids enable piping to occupy less volume in aircraft compared to the air ducts' volume. A good illustration of combination of these three systems is given in Figure 1.1 for the F-22 thermal management system. In this system,

there are two liquid cooling loops called forward loop and aft-ward loop, which contain polyalphaolefin (PAO) as coolant. The forward loop is responsible for the cooling of the mission-critical systems, and aft-ward loop is responsible for auxiliary systems that require liquid cooling. The air cycle system is also using the aft-ward loop as a heat sink. A vapor cycle cooling system is utilized between the liquid loops to transfer the heat from forward to aft-ward loop. The excess heat is transferred to fuel by a PAO to fuel heat exchanger and removed from aircraft by burning in engines. If the fuel temperature exceeds the limits, it is cooled by air-cooled fuel cooler.

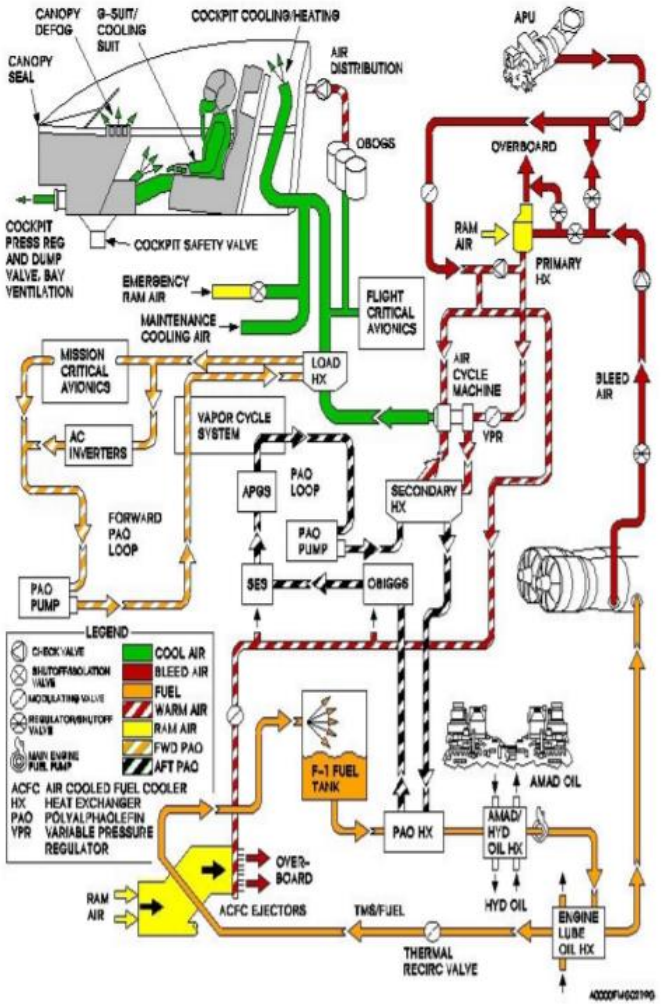

Figure 1.1. F-22 Thermal Management System [1]

The chips and modules in modern avionic devices are smaller in size but perform faster and better. This ongoing trend brings high power densities and high operational temperatures. If the heat removing rate stays behind the heat generation rate, residual heat causes the increase in the microprocessor temperature which in turn reduces the performance and reliability of the device. Increasing operating temperature causes an exponential increment in the failure rate of electronic devices. It is reported by U.S. Department of Defense [2] that the failure factor of electronic equipment increases exponentially with the increasing device temperature. In Figure 1.2, temperature dependent failure factor, which is the ratio of any temperature failure rate over failure rate at 75 ºC, exhibits an exponentially increasing trend with increasing temperature. Therefore, reliability of the equipment is directly correlated with the operating temperature.

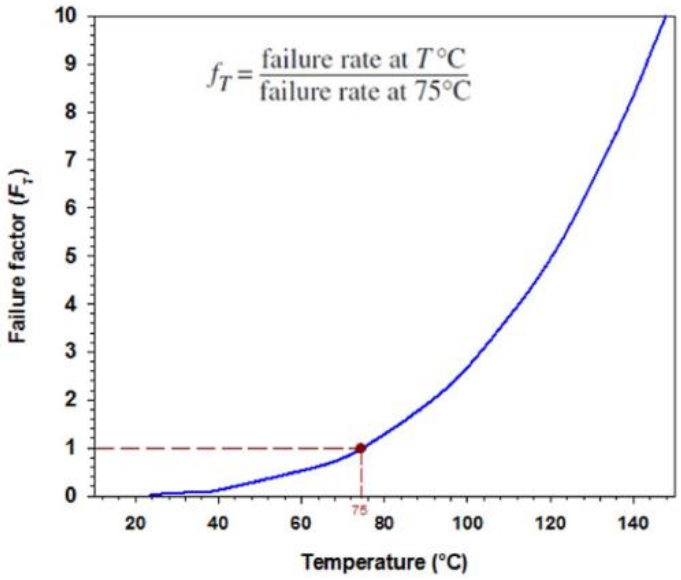

Figure 1.2. Temperature Dependent Equipment Failure Rate [2]

Because of the reduction in size and increase in performance, the power density of the components are increased. Increasing power density induces the need for an adequate cooling requirement. One of the areas where the high cooling demand emerges is

power electronics. It can be defined as the application of power semiconductor switches for controlling and converting electrical power efficiently. There are various applications of power electronics in various fields such as electrical appliances, robotic industry, electrical drives, more electric aircraft, etc. Most of the power electronic modules are cooled by a heat sink that is attached to the device. The heat sink is a passive heat exchanger that removes the generated heat from the device subjected to cooling to the cooling medium. Free and forced convection of air, forced convection of liquid, and liquid evaporation are the existing cooling modes for heat sinks. In Figure 1.3, a forced air-cooling application of a central processing unit (CPU) is illustrated.

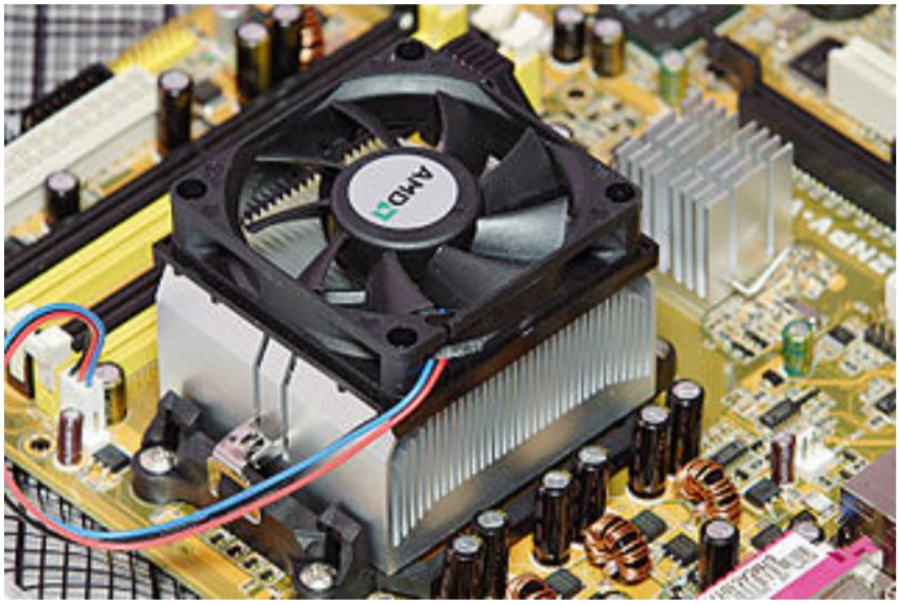

Figure 1.3. Forced Air Cooled CPU [3]

Higher packaging density of the electronic components leads to increase in generated heat flux. Therefore, the conventional heat sinks fail to deal with the high cooling demand of modern electronic equipment. Therefore, advanced cooling techniques have appeared to augment the heat removal rate. As emphasized before, if the proper

cooling is not provided, the failure rate of the equipment increases exponentially. Apart from conventional heat sink applications, in 1981, Tuckerman and Pease [4] showed that microchannels have a high heat dissipation capacity thanks to their high surface to volume ratio. The authors conducted single-phase water cooling experiments on a silicon microchannel substrate. It was seen that 790 W/cm^2 heat flux rate removal could be reached via 50 μm wide and 300 μm deep microchannels. This study showed that the microscale liquid cooling approach could cool the high heat generated electronic devices. Furthermore, remarkable decrease in the package size makes microchannel liquid cooling a promising technique.

The pioneering study of the Tuckerman and Pease paved the way for microchannel based liquid cooling studies to overcome the high-performance electronics, particularly integrated circuits' silicon chips. The next-generation military aircraft are expected to perform much better than the current aircraft's capability. Fighter aircraft superiority is directly related to its operational effectiveness. Operational effectiveness is determined based on aircraft specifications (low observability, flight performance), weapons configurations and detection capabilities (radar, electro-optic, electronic warfare systems, etc.). Increasing functionality and decreasing size of these detection items cause high power density. Increased power level becomes a crucial issue as the reliability of the equipment is a direct function of temperature levels of the component [5]. As a result, control of the electronics temperature is one of the design objectives during device development. This aim also encourages the development of alternative cooling approaches with higher reliability-cooling capacity.

Additionally, the occurrence of the different heat fluxes in printed circuit boards or chips is increased as the design complexity of the device goes further. The significant difference in heat flux causes hotspots. There can be single or several hotspots on the cooled subject, and the location of the hotspots may differ from application to application. In Figure 1.4, hotspot formation is illustrated which is caused by non-uniform power density along the Intel Pentium 3 processor die. It is stated that about 55% of the failure in electronic devices is induced by unequal thermal management

[6]. In addition to the temperature variation, the maximum junction temperature is vital for microprocessors. The upper limit of the junction temperature for the silicon microprocessors is expected to be maintained below 100 ºC [6]. If the maximum temperature limit is exceeded, the performance of the microprocessor is throttled to prevent total failure, so-called "protection mode". Performance loss of a mission-critical equipment in aircraft, such as radar, will be a crucial lost in a mission.

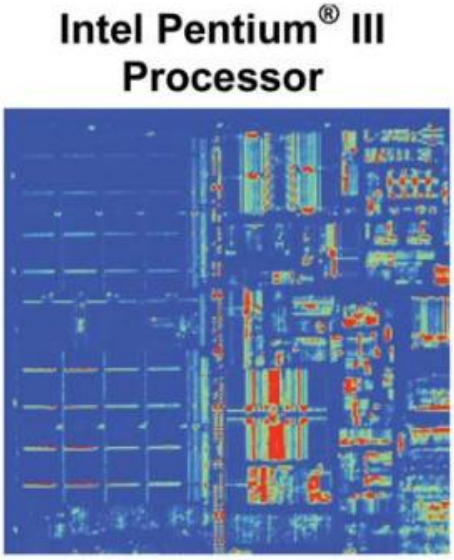

Figure 1.4. IR Image of on-die hotspots of Pentium 3 processor [7]

Microchannel heat sinks seem capable of cooling of the dense heat loads utilizing the high area to volume ratio. However, limitation at the micro-scale pumping power is one of the biggest challenges in microchannel research. Moreover, the flow regime remains in laminar range due to the small hydraulic diameters. There are several types of heat sinks, depending on fin geometry, orientation, and configuration. Depending on the application space consideration, heat load distributions, appropriate heat sink is selected. While designing the proper heat sink, there are several requirements to be considered:

- Lower thermal resistance
- Uniform temperature distribution
- Lower maximum temperature on the base surface
- Lower pumping power
- Higher compactness
- Lower fabrication cost

1.2. Literature Survey

Micro-electronic technology development continues to advance in conformity with the Moore's Law [8] which emphasizes while shrinking the feature sizes; the included transistor number doubles every year. In order to manage this increasing power and cooling demand, various cooling studies have been performed because the conventional cooling approaches fall behind the required performance criteria. The cooling modes can be classified into four categories which are:

- Radiation and free convection
- Forced air-cooling
- Forced liquid cooling
- Liquid evaporation

The applied cooling techniques are based on these cooling methods in different sizes and scales. The sequence of the cooling modes is given in the increasing effectiveness order. The approximate heat flux removing capabilities of the cooling modes are illustrated in Figure 1.5, considering the temperature difference between the ambient and heat transfer surface as 80 ºC. As effectiveness increases, the complexity of the method also increases. In this aspect, natural convection is preferred in low heat flux operations owing to simplicity, reliability, and low cost. Whenever the natural convection of air is not enough, forced convection is used. It is a reliable and low-cost method. It requires a fan for blowing the air through the cooling surface. However, its

cooling capacity is limited because of air. Forced convection of liquid cooling has higher heat transfer coefficient compared to the air cooling. Instead of fans, pumps are used for liquid flow. It has higher cost than forced air cooling due to fluid, pump, installation and maintenance issues. Liquid evaporation has the highest heat removal rate. It utilizes the enthalpy of vaporization. The pressure and temperature fluctuations may occur in the evaporation process which makes the design and maintenance critical. Due to high heating, installation, maintenance, fluids, and sustainability requirements, liquid evaporation has highest cost.

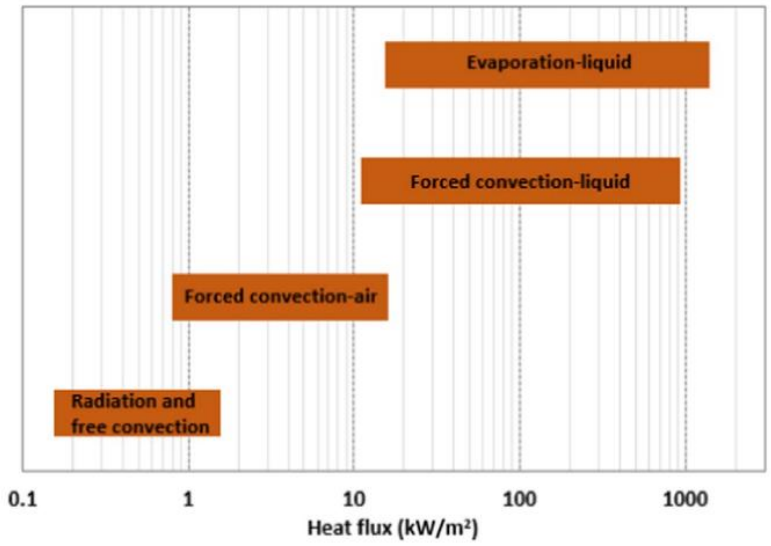

Figure 1.5. Heat flux comparison of conventional methods [9]

There are various emerging cooling techniques in the electronics cooling field. They can be classified into various types based on process adapted or effectiveness. Some of the well-accepted methods are as follows:

- Heat pipes
- Microchannels
- Spray cooling
- Phase change material cooling

The heat pipes have extensive application areas such as computers, laptops, telecommunication, and satellite modules. Heat pipe's working principle is based on the phase change of the working fluid inside the pipe. Accordingly, they do not have any moving parts which is the most remarkable feature of heat pipes. This feature provides the minimum maintenance necessity for heat pipes. The working principle of the heat pipes is described in Figure 1.6.

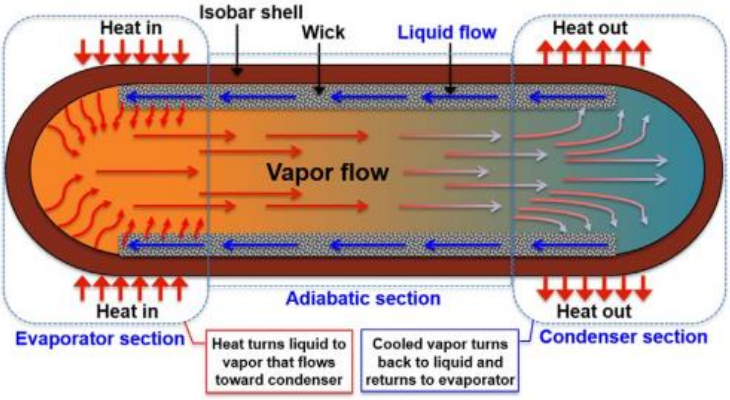

Figure 1.6. Heat pipe working principle [10]

The idea behind the use of microchannels is the increase in the area/volume ratio of the heat transfer devices. The air and various liquids can be used as coolant in microchannel applications. The most prevalent and low-cost coolant is water; however, the leakage is a reliability issue that can cause trouble for the electronic component. The spray cooling is an effective method of hotspot cooling. The coolant is sprayed on to the cooled surface. The liquid droplets evaporate when they get in contact with the surface. Like in the microchannel application, liquid contact with the electronic device is crucial point for spray cooling. Phase change materials are used where the cooling demand is not permanent but required in transients. A phase change material is used to absorb the peak energy and slowly rejects the heat in conjunction with the natural convection for a longer time. The melting point is critical when selecting the phase change material. The packaging, cooling method (fan-driven or

passive), operating temperature and the cost are significant criteria for designing a phase change material cooling system.

In addition to the mentioned cooling techniques, there is research on enhancing the properties of the cooling fluid by mixing the nanoparticles into the base fluid such as oxide ceramics (Al_2O_3), nitride ceramics (AIN), carbide ceramics (SiC), metals (Au, Ag), semiconductors (TiC2), carbon nanotubes and composite material. Nanofluids provide better thermal features such as thermal conductivity, convective, and boiling heat transfer performance with respect to base fluids; however, there are some issues to be solved like particle sedimentation, increased pressure drop, erosion, and fouling [11].

In their review, Kandlikar and Grande stated that the recent high-power electronics had been cooled by either evaporative cooling or impingement jet in hundreds of W/cm^2; however, the same values are reachable with single-phase laminar microchannel cooling [12]. In other words, single-phase microchannel cooling is still a comprising technique and in terms of complexity, it is more favorable than the evaporative or jet impingement techniques.

1.2.1. Microchannels

Since the pioneering work of Tuckerman and Pease [4], many researchers have been interested in the micro-scale cooling approach. The heat flux that Tuckerman and Pease were able to achieve was 790 W/cm^2, with a 71ºC temperature increase in the substrate with respect to the coolant fluid inlet temperature. They manufactured three geometries and tested them under different heat load conditions. The obtained thermal resistance was approximately 0.1 ºC/W, with approximately 210 kPa pressure drop.

Sadeghi et al. [13] pointed out that the shape of the microchannel cross-section area can affect the cooling performance, so they examined an annular cross-section channel with laminar forced convection. The inner wall temperature of the channel was kept

constant, and adiabatic boundary condition was applied on the outer wall. It was concluded that annular cross-section led to lower slip velocity, which resulted in a decrease in the exchange in the momentum at the solid/liquid interface, thus the heat transfer. They concluded that in the smooth channel, Nusselt number (Nu) decreases.

The shape of the channel cross-section was further investigated by Nonino et al. [14] for rectangle, trapezoidal, and hexagonal channels. Uniform wall heat flux and developing laminar flow were examined within specified cross-section shapes. It is discovered that temperature dependence of the viscosity should not be neglected since it has much influence on pressure drop. It was stated that channel shape influences the thermal performance but is not effective on pressure drop as well as viscosity.

The effect of surface roughness on thermal performance was investigated by Shokouhmand et al. [15] for a fully developed, laminar, rough rectangular microchannel. They used analytical Gaussian technique. The channels with 0 to 1 aspect ratio were examined while relative roughness was kept in between 0 and 0.15. It is seen that there is a strong relationship between the channel aspect ratio and the relative roughness. The heat transfer coefficient decreased when the relative roughness is decreased. Furthermore, the friction factor is increases with increasing relative roughness, as expected.

There are studies to enhance the cooling by using grooves on the microchannel walls. The idea behind using grooves is generating more disturbances in the flow to support a more effective cooling mechanism. In this context, Solovitz [16] took the two-dimensional grooves into consideration. He modified the groove depth, diameter and flow Reynolds number. He observed a 70% increment in the heat transfer while the pressure drop increase was only 30% when compared with a smooth channel with a Reynolds number of 1000 and aspect ratio of 0.4. There are also studies related to groove shape. Baghernezhad and Abouali [17] analyzed the groove's shape effect by comparing rectangular and arc-shaped grooves. Even though both grooves improve the cooling performance, arc-shaped was found to be more efficient. As a result, it was

found that grooves can improve thermal performance while sustaining the pressure drop.

The presence of micro pin-fins is also an effective way in the improvement of the microchannel heat transfer. Pin-fins enhance the heat removal by increasing the surface area and disrupting the steady fluid flow. In the literature, it is seen that a wide variety of pin-fins with different shapes, sizes, and arrangements have been utilized to improve thermal performance. Vanapalli et al. [18] analyzed the different pin-fin shapes and compared thermohydraulic performance for nitrogen gas flow in micro channel. The tested pin-fin cross-sections were square, circle, elliptic, rhombus, sine-shaped and eye-shaped. They tested in staggered arrangement. The researchers stated that fin shapes affect the flow so when the fin shape does not disturb the flow, the less separation occurred. The decreased separation created less thermal resistance.

Generating secondary flow along the channel is another way to enhancing the heat transfer in microchannels. Lee et al. [19] introduced the usage of oblique fins for the laminar microchannel flow to examine its heat transfer and pressure drop performance numerically. The channel geometry can be called modified conventional microchannel since oblique openings implemented the regular channel as shown in Figure 1.7. The interruption of the continuous fins into the oblique fins also induces the re-development of the thermal boundary layers and reduces boundary layer thickness. The flow is kept in developing state so results in better thermal performance in the channel. The heat transfer coefficient of the oblique finned channel improved by 80% compared to the conventional channel. The increase in the pressure drop was reasonable considering the heat transfer enhancement.

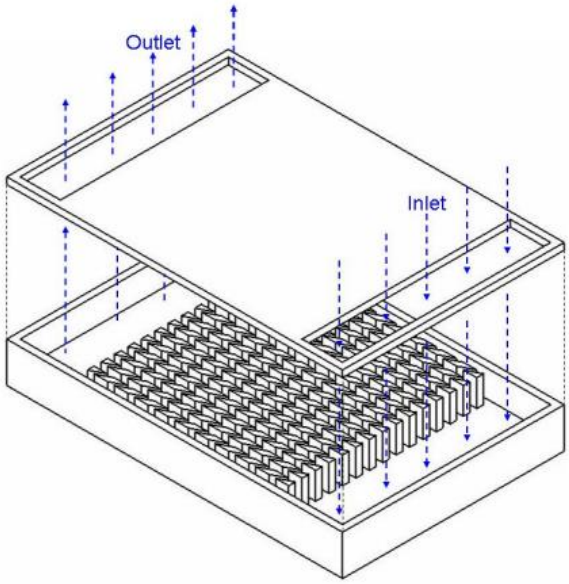

Figure 1.7. Isometric view of the micro channel heat sink with oblique fins [19]

In terms of the material of the heat sink, thermal conductivity of the heat sink is a crucial factor for the thermal performance. The higher thermal conductivity provides lower thermal resistance, so the lower temperature along with the heat sink. Zhong et al. [20] studied the effect of varying properties such as fluid speed, heating power, micro-fin structures, and thermal conductivity. It is found out that with high thermal conductivity material, heat transfer can be enhanced significantly while keeping the pressure drop quite constant.

Brunschwiler et al. [21] benchmarked thermal management performances of three topologies in three-dimensional chip stack cooling. They are illustrated in Figure 1.8. The presence of thermal interface materials accounts for a critical portion of the thermal resistance. In that respect, embedded microchannels into the backside of die remove the thermal interface materials and simplify the thermal path. However, embedded cooling is required to have leakproof fluid interconnects from cooling loop to the chip stack. It is stated that embedded cooling showed the best thermal performance.

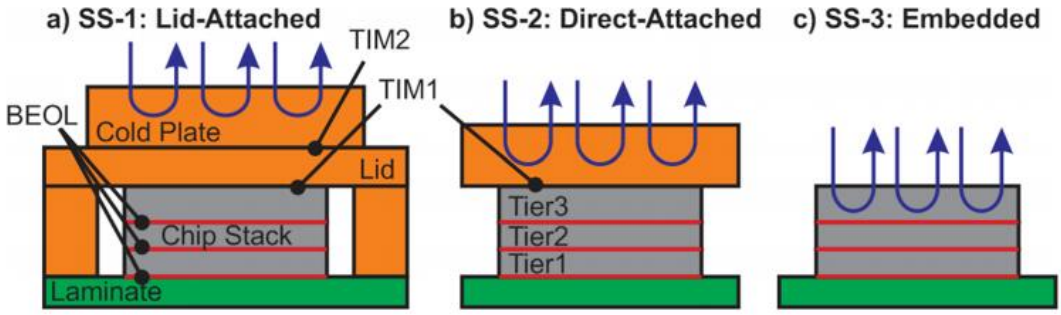

Figure 1.8. 3D chip stack thermal management landscape [21]

One of the critical problems for the cooling studies is the occurrence of the localized hotspots within the component, resulting in high temperatures, which leads to diminished functioning of the device. Rubio-Jimenez et al. [22] introduced a numerical study of variable pin fin density clustering along the microchannel in order to obtain a more uniform temperature distribution with reduced pressure drop compared to the uniform clustered pin fins. The fin length, fin height, fin shape, longitudinal pitch, and transversal pitch were some of the critical parameters that were analyzed. It was observed that variable fin density is successful for decreasing the overall temperature gradient than the uniformly distributed fins.

Sarvey et al. [23] compared the effectiveness of non-uniform micro pin fin clustering experimentally with four different specimens. The cylindrical and hydrofoil shaped pin fins are employed. The fins were located around the hotspot clustered in two different configurations, which are spanwise and local as shown in Figure 1.9. The hot spot heat flux of 500 W/cm^2 and background heat flux of 250 W/cm^2 are applied. The results showed that in order to lower the hotspot temperature, spanwise clustering of hydrofoil fins showed better performance than others.

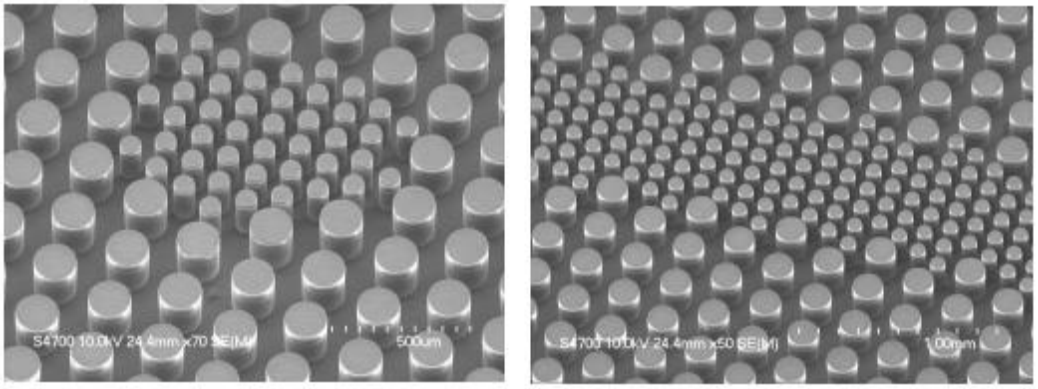

Figure 1.9. Local pin clustering (left) and spanwise pin clustering (right) [23]

Kandlikar and Lorenzini-Gutierrez [24] performed a numerical study, in order to mitigate the temperature nonuniformity on the 3D integrated circuit application where the height restriction is 100 μm. By employing offset strip fins with variable fin density, they aimed not only lowering the temperature variation but also obtaining a relatively low temperature. The working chip had a dissipation of 200 W and 1 cm^2 surface area. At the end of the study, it is revealed that with variable offset strip fins, remarkable performance development can be obtained. Another important outcome of the study was that taking the dynamic fluid viscosity as constant may lead significant overestimation of the pressure drop.

1.2.2. Microchannel Optimization

Many types of research have been performed on the micro-scale cooling to understand the heat transfer and pressure drop characteristics. While doing the studies, randomly generated geometries have been used mostly. Li and Peterson [25] performed a three-dimensional conjugate heat transfer study for a parallel microchannel heat sink numerically and optimized it. They compared the results with the initial experimental results of the Tuckerman and Pease [4] and claimed that optimized geometry performed 20% improved under the same operating conditions.

In the literature, there were many optimization schemes utilized by the researchers to obtain an optimized geometry for microchannel heat sink applications. The initial optimization studies were done with numerical tools such as the Lagrangian polynomial method in the early stages of this field of study [26]. Afterward, evolutionary optimization algorithms were introduced in this subject. Single-objective and multi-objective evolutionary algorithms, such as the Sequential Quadratic Programming Algorithm (SQP) [27] and Non-Dominated Sorting Genetic Algorithm (NSGA-II) were employed [28], assured a successful performance. There are many other algorithms, such as Multi-objective Genetic Algorithm (MOGA), Goal Attainment Algorithm (GAA), and Strength Pareto Evolutionary Algorithm (SPEA2) that are used for microchannel optimization studies in the literature.

Abdelsalam et al. performed a multi-objective genetic algorithm (MOGA) optimization approach on plate-fin heat sink applications for data centers and telecommunication systems [29]. The goal was improving the heat dissipation performance of the heat sinks by optimizing the geometric parameters like orientation, shape, and number of fins of the plate-fin heat sink. They follow an approach that the initial population is generated with MOGA and analyzed on ANSYS. After first iteration is solved and best candidates are selected, second generation is generated and the again analyses are done. This process carries on until the optimum configuration is obtained. They carried on this loop eighteen times and reported that between 11.2% and 18.1% effectiveness increase in heat dissipation is obtained compared to the baseline heatsinks set as benchmark.

Andersson T. et al. developed a simulation-optimization framework for a conjugate heat transfer model of a plate heat sink [30]. The model consists of three main components, which are a conjugate heat transfer solver, a CAD generator, and optimization control. FreeCAD was used as the CAD generator and MATLAB as the optimization controller. Lastly, IPS IBOFlow was the last element of the chain as conjugate heat transfer solver. They tried to set a framework for optimizing the pressure drop, thermal resistance, and the power consumption for air blowing. They

implemented an automatic volume generation technique by employing immersed boundary method. Immersed boundary helps to differ the fluid cells and the solid cell to define the boundary and interface between fluid and solid domains. Sandwiching algorithm solves the weighted sum problems consecutively until the resulting Pareto solutions include the Pareto front so that Pareto points are close to the Pareto front.

Türkakar [31] performed an analytic optimization study for silicon microchannel heat sinks. In this study, eight different metal-polymer microchannel heat sinks were analyzed to create a general understanding of the heat sinks' heat removal capabilities under the 85ºC temperature constraint and constant pumping power implementation. The optimization of these eight cases was done considering the minimization of the thermal resistance as objective function. Additionally, a CPU heat sink optimization was performed while considering copper and silicon as heat sink materials. In another study, Türkakar and Okutucu [32], enhanced the previous model to investigate the optimization of the microchannel heat sink with the presence of hotspots. The same CPU application is considered, but instead of uniform heat flux, equivalent four different hotspots were considered with pumping power and maximum temperature constraints. The achieved highest temperature of the optimized heat sink was 48.9ºC, which is far below the critical value of 85ºC.

1.2.3. Response Surface Method & Design of Experiments

Response surface method (RSM) simplifies complex engineering simulations into surrogate models by using the outcomes of simulated domain or physical experiments defined by the design of experiments (DOE). It is comprised of mathematical and statistical methods that contribute to the model and analyze problems in which an objective function is affected by several parameters. Usage of the surrogate models makes understanding the relationship easier between the design parameters and response metrics. It makes the evaluation of new designs possible in the considered design range but does not perform well out of the range. Robinson et al. [33]

categorized the surrogate models into three categories based on their mathematical structure. The response surface method is classified as a data-driven surrogating method and the other categories which are projection-based methods and multi-fidelity-based surrogating. Detailed study related to surrogate models investigated in [34].

Response surface methods vary from Least Square approaches to stochastic methods. Compared to the other approaches, the second-order quadratic model is found to be more appropriate where curvature behavior of the response is observed, which is more probable in real-world problems. The second-order model is also more flexible and easy for estimation of the coefficients [35]. The general expression of the second-order equation is

$$y = \beta_0 + \sum_{i=1}^{k} \beta_i x_i + \sum_{i=1}^{k} \beta_{ii} {x_i}^2 + \sum_{i=1}^{k} \sum_{j=1}^{k} \beta_{ij} x_i x_j + \varepsilon \qquad (1.1)$$

where x and y indicate design variables and response, respectively. The terms β and ε stand for equation coefficients and numerical error.

RSM is completely related to the DOE. The approach is using the outcomes of a DOE run for creating an approximation of the response variable through the design space. The response surface is an analytical function of specified design variables, so the optimization of that function is high-speed. However, if the design space expedition is ineffective, the result of the response surface assisted optimization can be irrelevant from the actual case because of the unfavorably estimated model coefficients.

There are various DOE techniques available such as randomized complete block design, Latin square, full factorial, fractional factorial, central composite design, Box-Behnken, Plackett-Burman, Taguchi, Random, Halton-Faure, Latin Hypercube, and others [36]. Each technique has its design space exploration logic. While choosing the appropriate method, it must be considered that if the experiments are time-consuming and costly, reduced number of experiments is favorable. In this aspect, the Central Composite Design (CCD) reduces the number of experiments since it is a sequential

design method. It is the combination of 2^k full factorial to which the central point and star points are added. Star points are the center points for each design surface [37].

In some practical situations, while specifying the design variables, ranges of the design variables can be strict, especially in the engineering applications. This design space is called a cuboidal design. The design points cover the limits of the experimental region. It is often called as face-centered cube since the axial points are located at the center of the faces rather than outside of the faces. The axes represent the design variables in Figure 1.10. The face-centered cube design is suitable for any number of design variables [35].

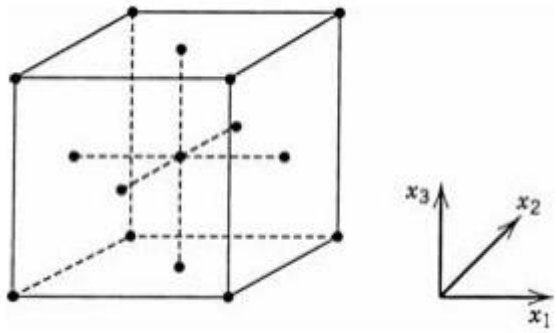

Figure 1.10. Face centered cube [35]

Kant conducted a modelization and optimization study using CFD and response surface methodology to analyze the fluid flow and heat transfer via different manifold shapes [38]. Four different manifolds are studied. Four operating conditions are inspected, which are channel width, depth, spacing, and inlet Reynolds number. The response surface is employed to optimize the operating conditions of different microchannel systems. The computational domain is assumed to be steady, laminar and incompressible flow. Simulations are conducted in Ansys-Fluent environment. In order to generate response surface equations, central composite design point attained. According to outcomes of the response surface ANOVA study, they revealed that channel width is most governing parameter on pressure drop.

Chiang et al. [39] performed an optimization study of a pin fin heat sink experimentally by employing RSM. Pin fin height, diameter, and width of pitch between fins were designated as design parameters. Experiment design points were specified with central composite design. The surrogate models for thermal resistance and pressure drop were generated and optimized with sequential approximation optimization method. At the end of the study, researchers run three confirmation experiments to compare the predicted and experimental values. It was seen that the percentage error between the predicted and actual value of thermal resistance and pressure drop lies within -5.1% to 2.2% and -4.1% to 2.4%, respectively. It was observed that experimental values are within 95% of the prediction interval.

1.3. Motivation and Objectives

Fighter aircraft superiority is directly related to its operational effectiveness. Operational effectiveness is determined based on aircraft specifications (low observability, flight performance), weapon configurations, and detection capabilities (radar, electro-optic, electronic warfare systems, etc.). Increasing functionality and decreasing size of these detection items cause high power density. Increased power level becomes crucial issue as the reliability of the equipment is a direct function of temperature levels of the component [5]. As a result, control of the electronics temperature is one of the design objectives for heat sink design. This aim also encourages the development of advanced cooling approaches with higher functionality. Accordingly, single-phase liquid cooling heat sink in micro-scale serves this purpose. The pioneering work of Tuckerman and Pease [4] showed that heat fluxes around 1000 W/cm^2 could be removed by microchannel application.

As the power density of high-performance device increases, lowering the maximum temperature become a significant concern. The presence of concentrated high-power regions (hotspots) is a challenging issue in terms of lowering the temperature. The uniformly distributed pins or channels provide equal heat removing rate for all

regions; however, at the hotspots, heat removing capacity falls behind the required cooling demand. In this case, temperature of the hotspots exceeds the structural limits and causes failure. The necessity of non-uniformly clustered fins or channels come into view at this point. These designs can provide high cooling demand at the hotspots and moderate cooling rates in the background areas. However, while designing a non-uniform heat sink, pressure drop performance should also be considered.

The main objective of this study can be summarized as:

- Selection of the operating conditions of the heat sink and performing preliminary calculations.
- Determination of the hotspot cooling method.
- Predicting the pressure drop and thermal resistance by using computational fluid dynamics (CFD) for determined fin-type through performing the design of experiment (DOE) and response surface method (RSM).
- Finding the optimized geometry for given conditions.
- Comparing the resulting geometry with the literature.

1.4. Present Study

The present study has an optimization approach. First chapter includes the literature research about the micro-scale cooling, optimization, and response surface methodology. It aims to create a general understanding for the micro-scale cooling approaches and micro-scale cooling enhancement studies. Moreover, some optimization studies and information about the response surface method are presented. Afterwards, motivation and objectives of the study are stated. Chapter 2 contains the method of approach for the current study. Cross section shape selection of the fin is determined first. Governing equations and assumptions are presented. Then, heat sink optimization approach is clarified with response surface method. Heat sink optimization is done in Chapter 3. Heat sink geometry and heat load conditions are

defined. Then, fixed and varying dimensions are introduced. After the varying dimensions are specified, design space for the experimental runs is created with DOE method, in order to understand and predict second order response surface equations for the pressure drop and thermal resistance. To be able to conduct CFD studies, validation study is performed. Once the validated model is acquired, response surface equations are obtained, and design parameters effects are discussed. Finally, multi-objective optimization with genetic algorithm is performed for two objective functions which are minimization of the thermal resistance and pressure drop. Most suitable optimum solution is selected with the help of Technique for Order of Preference by Similarity to Ideal Solution method. Lastly, predicted optimum solution results are compared with CFD analysis results.

The main contribution of the present study is that a design methodology has been established for variable clustering of the fins in the presence of hotspot for a T/R module.

CHAPTER 2

METHOD OF APPROACH

2.1. Fin Selection

In terms of mitigating the hotspot temperature, it is seen that most researchers concentrate on specific fin types, which are generally pin fins, wavy fins, and oblique fins. The highest heat flux removing capabilities of these fins, found in literature, are compared in Table 2.1.

Table 2.1. Fin type comparison

Fin Type	Maximum Heat flux [W/cm^2]
Pin fin [23]	500
Oblique fin [40]	400
Wavy fin [41]	300

Decreasing the maximum hotspot temperature is a critical issue, so pin fins are decided to be assessed in this study.

For the pin fin cross-section shape, there are a variety of possibilities [42] such as circular, hydrofoil, cone-shaped, rectangular, etc. In order to simplify the current study and since cross-section of the pin fin is not the focus of the study, circular pin fin is selected.

In the literature, spanwise clustering (see Figure 1.9) is superior in terms of providing the homogenized flow resistance in the transverse direction. In contrast, if the pin fin clustering is done locally, the bypass effect occurs, and less fluid will flow over the hotspot, which will result in higher hotspot temperature [43]. Consequently, spanwise pin fin clustering at the hotspot region is preferred here.

Pin fins may have two different arrangements, which are inline and staggered. Incropera and DeWitt [44] states that the staggered arrangement is favorable for enhancing the heat transfer. Therefore, staggered arrangement is preferred.

2.2. Design of Experiments

As pointed out in Section 2.1, circular pin fin is interpreted as a suitable fin type for cooling of the electronic equipment with a hotspot. Four continuous parameters and one discrete parameter are selected for circular pin fin as design parameters, which are fin diameter, fin pitch, hotspot fin array length, fin height, and fluid inlet velocity, respectively. Except for the hotspot fin array length, remaining four parameters have strong influence on the performance of heat sink [45]. Considering the DOE methods, Anderson and Whitcomb [46] pointed out that CCD ensures a strong foundation for generating a response surface map. By using the commercial software MINITAB, design space is created. The created design space is given in Table 2.2. The columns A, B, C, D stand for the continuous variables: fin diameter, fin pitch, hotspot fin array length, and fin height, respectively. Column E stands for the discrete parameter, which is fluid inlet velocity. -1, 0, and 1 denote the minimum, midpoint and maximum values in the A, B, C, D columns for corresponding variables, respectively. In column E, three different fluid velocities are denoted with 1, 2, and 3.

Table 2.2. Design Space

RunOrder	A	B	C	D	E
1	-1	-1	-1	-1	1
2	1	-1	-1	-1	1
3	-1	1	-1	-1	1
4	1	1	-1	-1	1
5	-1	-1	1	-1	1
6	1	-1	1	-1	1
7	-1	1	1	-1	1
8	1	1	1	-1	1
9	-1	-1	-1	1	1

Table 2.2. (Continued)

RunOrder	A	B	C	D	E
10	1	-1	-1	1	1
11	-1	1	-1	1	1
12	1	1	-1	1	1
13	-1	-1	1	1	1
14	1	-1	1	1	1
15	-1	1	1	1	1
16	1	1	1	1	1
17	-1	0	0	0	1
18	1	0	0	0	1
19	0	-1	0	0	1
20	0	1	0	0	1
21	0	0	-1	0	1
22	0	0	1	0	1
23	0	0	0	-1	1
24	0	0	0	1	1
25	0	0	0	0	1
26	-1	-1	-1	-1	2
27	1	-1	-1	-1	2
28	-1	1	-1	-1	2
29	1	1	-1	-1	2
30	-1	-1	1	-1	2
31	1	-1	1	-1	2
32	-1	1	1	-1	2
33	1	1	1	-1	2
34	-1	-1	-1	1	2
35	1	-1	-1	1	2
36	-1	1	-1	1	2
37	1	1	-1	1	2
38	-1	-1	1	1	2
39	1	-1	1	1	2
40	-1	1	1	1	2
41	1	1	1	1	2
42	-1	0	0	0	2
43	1	0	0	0	2
44	0	-1	0	0	2
45	0	1	0	0	2
46	0	0	-1	0	2
47	0	0	1	0	2

Table 2.2. (Continued)

RunOrder	A	B	C	D	E
48	0	0	0	-1	2
49	0	0	0	1	2
50	0	0	0	0	2
51	-1	-1	-1	-1	3
52	1	-1	-1	-1	3
53	-1	1	-1	-1	3
54	1	1	-1	-1	3
55	-1	-1	1	-1	3
56	1	-1	1	-1	3
57	-1	1	1	-1	3
58	1	1	1	-1	3
59	-1	-1	-1	1	3
60	1	-1	-1	1	3
61	-1	1	-1	1	3
62	1	1	-1	1	3
63	-1	-1	1	1	3
64	1	-1	1	1	3
65	-1	1	1	1	3
66	1	1	1	1	3
67	-1	0	0	0	3
68	1	0	0	0	3
69	0	-1	0	0	3
70	0	1	0	0	3
71	0	0	-1	0	3
72	0	0	1	0	3
73	0	0	0	-1	3
74	0	0	0	1	3
75	0	0	0	0	3

2.3. Computational Fluid Dynamics

A numerical solution is preferred due to several advantages: it is a time-saving method compared with the experimental approach. Also, the numerical approach saves time

in design and optimization stages and lowers the cost due to time-consuming microfabrication processes.

The numerical model is a conjugate heat transfer problem. In the model, the following assumptions are made:

1. The flow is steady-state, laminar, and incompressible.
2. Radiation is neglected.
3. Temperature dependent solid property (thermal conductivity) and fluid property (dynamic viscosity) are employed. The remaining thermophysical properties are constant.
4. Viscous dissipation is negligible.
5. Body forces neglected.

Based on the prevailing assumptions, the conservation of mass and momentum equations for the fluid domain are reduced to,

$$\left(\frac{\partial u}{\partial x}+\frac{\partial v}{\partial y}+\frac{\partial w}{\partial z}\right)=0 \tag{2.1}$$

where u, v, w are the x, y, z velocity components of flow.

$$\rho\left(u\frac{\partial u}{\partial x}+\ v\frac{\partial u}{\partial y}+w\frac{\partial u}{\partial z}\right)=-\frac{\partial P}{\partial x}+\mu\left(\frac{\partial^2 u}{\partial x^2}+\frac{\partial^2 u}{\partial y^2}+\frac{\partial^2 u}{\partial z^2}\right) \tag{2.2}$$

$$\rho\left(u\frac{\partial v}{\partial x}+\ v\frac{\partial v}{\partial y}+w\frac{\partial v}{\partial z}\right)=-\frac{\partial P}{\partial y}+\mu\left(\frac{\partial^2 v}{\partial x^2}+\frac{\partial^2 v}{\partial y^2}+\frac{\partial^2 v}{\partial z^2}\right) \tag{2.3}$$

$$\rho\left(u\frac{\partial w}{\partial x}+\ v\frac{\partial w}{\partial y}+w\frac{\partial w}{\partial z}\right)=-\frac{\partial P}{\partial z}+\mu\left(\frac{\partial^2 w}{\partial x^2}+\frac{\partial^2 w}{\partial y^2}+\frac{\partial^2 w}{\partial z^2}\right) \tag{2.4}$$

where ρ is the fluid density, P is the pressure vector, μ is the dynamic viscosity.

The energy conservation equation for the fluid domain is,

$$\rho C_p \left(u \frac{\partial T}{\partial x} + v \frac{\partial T}{\partial y} + w \frac{\partial T}{\partial z} \right) = k_f \left(\frac{\partial^2 T}{\partial x^2} + \frac{\partial^2 T}{\partial y^2} + \frac{\partial^2 T}{\partial z^2} \right) \tag{2.5}$$

where C_p is the specific heat, k_f is fluid thermal conductivity.

For the solid domain, the heat diffusion equation is,

$$\frac{\partial}{\partial x}\left(k_s \frac{\partial T}{\partial x} \right) + \frac{\partial}{\partial y}\left(k_s \frac{\partial T}{\partial y} \right) + \frac{\partial}{\partial z}\left(k_s \frac{\partial T}{\partial z} \right) = 0 \tag{2.6}$$

where k_s is the solid thermal conductivity.

2.4. Response Surface Methodology

Once the numerical analyses of all created experimental points are done, obtained pressure drop and thermal resistance data are used as input for creating the response functions, as described in Section 1.2.3. The regression coefficients are estimated by the outcomes of the DOE analyses by the method of least squares [35]. This process is done with MINITAB software.

2.5. Optimization

The optimization of the heat sink is constructed as a multi-objective optimization problem, which can be summarized as;

$$\begin{gathered} \min \vec{f}(\vec{x}) = [f_1(\vec{x}), f_2(\vec{x})] \\ subject\ to\ g_1(\vec{x}) \leq a\ , g_2(\vec{x}) \leq b\ and\ c \leq g_3(\vec{x}) \leq d \end{gathered} \tag{2.7}$$

where $\vec{x}$ is the design variables vector, $\vec{f}$ is the design objectives vector and g_1, g_2, g_3 are the design constraints. As a result of the multi-objective optimization process, a non-dominated solution set is obtained, which is called Pareto front [47]. In this study, minimization of the thermal resistance and minimization of the pressure drop are the design objectives. The constraints are maximum pressure drop, maximum silicon temperature and pumping power interval which are defined according to available literature data. The optimization process is performed on Matlab's optimization tool. The working scheme of the genetic algorithm is given in Figure 2.1.

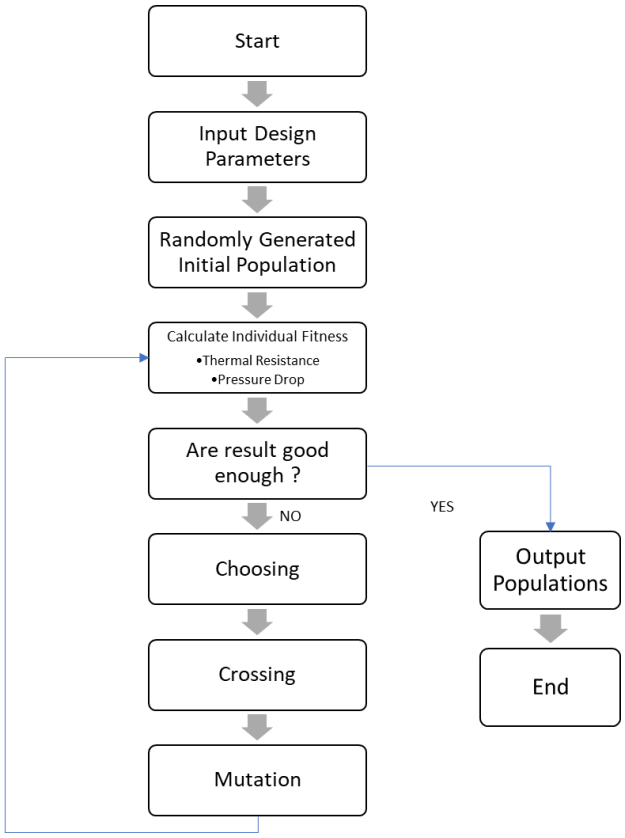

Figure 2.1. Genetic Algorithm Scheme

CHAPTER 3

DESIGN OPTIMIZATION STUDIES

3.1. Introduction

In this chapter, the studied problem is described, and solution methodology is explained. As stated previously, modern fighter aircraft have advanced flight and mission systems. The availability of this equipment is critical. It is seen that heat flux in the range of 120-600 W/cm^2 is already available in the field [48]. In terms of total heat load, Revankar et al. [49] stated that T/R modules could reach a maximum heat dissipation of 500 W.

3.2. Geometry

Because of the lack of information about the T/R module, the geometry of the heat sink is developed in consistent with the literature.

3.2.1. Fixed Dimensions

The heat sink dimensions are designated as 8 × 32 × 0.4 mm^3 based on literature [50]. The heat flux is applied on an 8 × 25 mm^2 area on which the pin fins are constructed. Because of the embedded cooling concept, base thickness is taken as 100 μm, so the channel height is 300 μm. The hotspot area is defined at the center of the heat sink with 1000 × 1000 μm^2 area. The geometry of the heat sink is shown in Figure 3.1 and Figure 3.2. The relationship between the background and hotspot pin fin diameters is

$$d_{bg} = 2\, d_{hs} \tag{3.1}$$

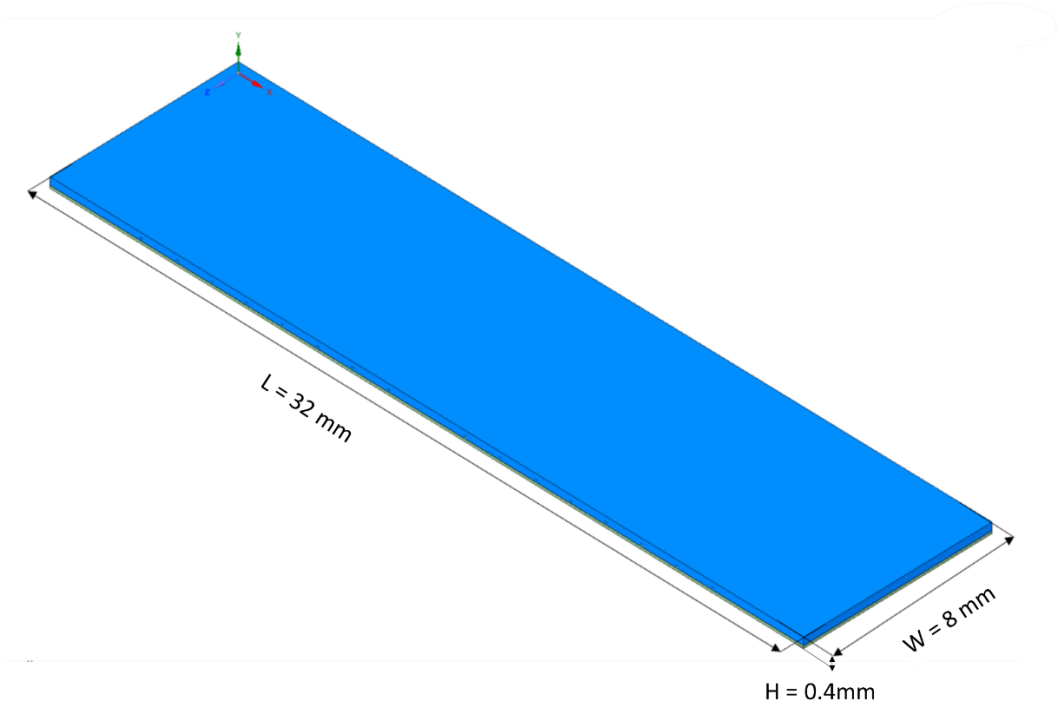

Figure 3.1. Heat sink base dimensions

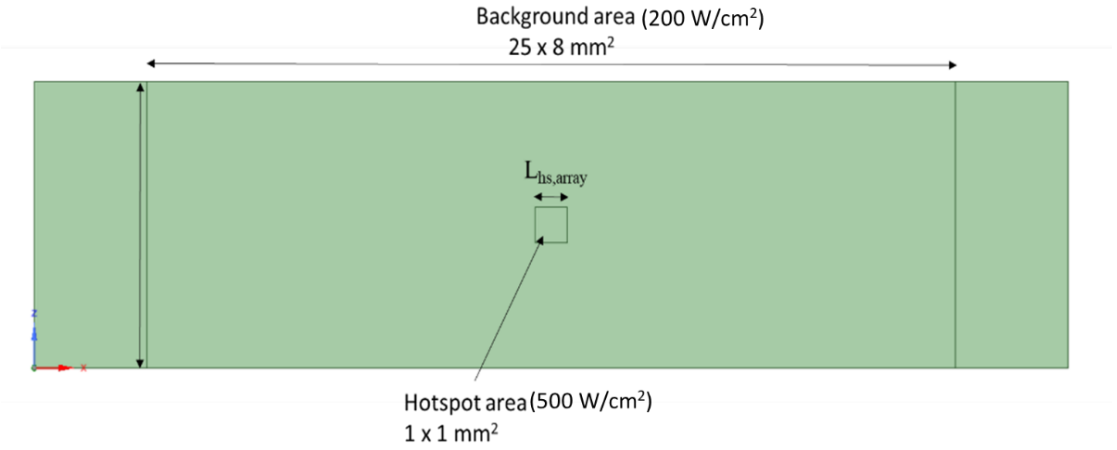

Figure 3.2. Background and Hotspot heat flux areas

3.2.2. Varying Dimensions

In order to optimize the hydrodynamic and thermal performance of the heat sink, four different geometric parameters and mass flow rate are determined. In order to evaluate the performance of the heat sink in laminar range Reynolds numbers, analyses are done with three inlet velocities 0.847, 1.27 and 1.693 m/s. The chosen design variables are fin diameter, fin pitch ratio, hotspot fin array length, and fin height. The design variables and their ranges are listed in Table 3.1. In the table, for the specified flow inlet velocities, corresponding mass flow rates are given.

There are different approaches for defining the Reynolds number in the presence of pin fins. There are studies in which the Reynolds number is defined based on pin-fin diameter [50,51] and based on channel/duct hydraulic diameter [53]. In this study, the hydraulic diameter is defined as the ratio of the open duct volume available for flow to wetted surface area inside the heat sink [54]. This approach is found appropriate because there are a wide variety of configurations to be investigated in this work.

$$d_{hyd} = \frac{4V_f}{A_f} \tag{3.2}$$

Here V_f is total fluid volume in the heat sink. A_f is the wetted surface area, which is the surface area in contact with the fluid.

The shape of the duct in which the fluid flows through is a rectangle with width W, height H, length L, pin fin section area A_p, pin fin circumference length L_p, and number of pin fins N. Therefore, the total fluid volume and wetted surface area are determined as below.

$$V_f = WHL - NA_pH \tag{3.3}$$

$$A_f = 2(W + H)L + N(L_p H - 2A_p) \tag{3.4}$$

The equations (3.3) and (3.4) are applicable for uniform clustered circular pin fins. Therefore, from Table 3.2, the maximum and minimum hydraulic diameters are calculated for created experimental points. Since the geometries in this study have densely clustered pin fin section, to be more practical, CAD program Spaceclaim is used for measuring the volume and area properties. It is seen that the maximum and minimum hydraulic diameters for the created geometries are 518 μm and 137 μm, respectively.

The Reynolds number is

$$Re = \frac{\rho u_{inlet} d_{hyd}}{\mu} \tag{3.5}$$

In order to investigate the Reynolds number range, Eqn. (3.5) is used with the available data, hydraulic diameter, and inlet flow velocity ranges. Since the water is assumed incompressible, with constant density of 997 kg/m^3, and inlet dynamic viscosity is taken as 0.0009764 Pa.s. Corresponding design variables data is given in Table 3.1. In the table, inlet velocities are converted corresponding mass flow rate values. It is seen that Reynolds number varies between 118 and 895. It is stated that, with the presence of micro pin fins and Reynolds number beyond the 100-300 range, flow transitions from steady laminar flow to vortex shedding regime [23]. Since the Reynolds numbers in this study are within or beyond this range, vortex shedding is expected.

Despite the available small characteristic lengths and Reynolds number values, flow is subjected to conventional Navier Stokes and energy conservation equations since the characteristic length of the channel is significantly larger than the mean free path of the liquid water molecules. Qu and Mudawar [55] stated for the applications with characteristic length greater than 100 μm and Reynolds number below 1700, conventional Navier Stokes equations are applicable.

Hotspot fin array length is one of the design parameters to be investigated in this study. It is shown in Figure 3.3 , which is bottom view of the halved geometry.

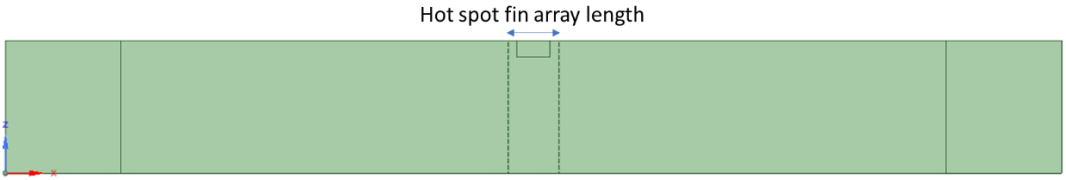

Figure 3.3. Hotspot fin array length

Transverse and longitudinal pitch are kept constant for background and hotspot fins. The relationship between the pitch ratio and the pin diameter is

$$Pitch\ Ratio = \frac{S}{d} \tag{3.6}$$

where S stands for both longitudinal and transverse pitch, d is the diameter of circular pin. The longitudinal and transverse pitch are shown in Figure 3.4, where longitudinal pitch is in the flow direction.

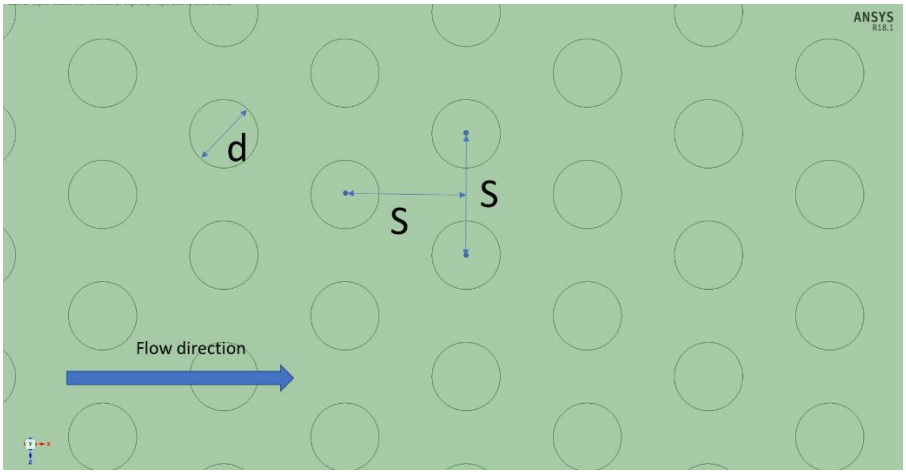

Figure 3.4. Longitudinal and transverse pitch

Table 3.1. Design variables

Water mass flow rate	0.00101-0.00201kg/s
Fin eight	100-300 μm
Fin diameter	200-500 μm
Pitch ratio	1.5-2
Hotspot fin array length	1000-2000 μm

3.3. DOE

The experimental setup is obtained with the CCD method for specified design variables. The extremum points are indicated. Table 3.2 summarizes the created design space.

Table 3.2. DOE setup

Diameter(μm)	Pitch Ratio	HS Length(μm)	Fin Height(μm)	mass flow rate[kg/s]
200	1.5	1000	100	0.00101
500	1.5	1000	100	0.00101
200	2	1000	100	0.00101
500	2	1000	100	0.00101
200	1.5	2000	100	0.00101
500	1.5	2000	100	0.00101
200	2	2000	100	0.00101
500	2	2000	100	0.00101
200	1.5	1000	300	0.00101
500	1.5	1000	300	0.00101
200	2	1000	300	0.00101

Table 3.2. (Continued)

Diameter(μm)	Pitch Ratio	HS Length(μm)	Fin Height(μm)	mass flow rate[kg/s]
500	2	1000	300	0.00101
200	1.5	2000	300	0.00101
500	1.5	2000	300	0.00101
200	2	2000	300	0.00101
500	2	2000	300	0.00101
200	1.75	1500	200	0.00101
500	1.75	1500	200	0.00101
350	1.5	1500	200	0.00101
350	2	1500	200	0.00101
350	1.75	1000	200	0.00101
350	1.75	2000	200	0.00101
350	1.75	1500	100	0.00101
350	1.75	1500	300	0.00101
350	1.75	1500	200	0.00101
200	1.5	1000	100	0.00151
500	1.5	1000	100	0.00151
200	2	1000	100	0.00151
500	2	1000	100	0.00151
200	1.5	2000	100	0.00151
500	1.5	2000	100	0.00151
200	2	2000	100	0.00151
500	2	2000	100	0.00151
200	1.5	1000	300	0.00151
500	1.5	1000	300	0.00151
200	2	1000	300	0.00151
500	2	1000	300	0.00151
200	1.5	2000	300	0.00151
500	1.5	2000	300	0.00151
200	2	2000	300	0.00151
500	2	2000	300	0.00151
200	1.75	1500	200	0.00151
500	1.75	1500	200	0.00151
350	1.5	1500	200	0.00151
350	2	1500	200	0.00151
350	1.75	1000	200	0.00151
350	1.75	2000	200	0.00151
350	1.75	1500	100	0.00151
350	1.75	1500	300	0.00151

Table 3.2. (Continued)

Diameter(μm)	Pitch Ratio	HS Length(μm)	Fin Height(μm)	mass flow rate[kg/s]
350	1.75	1500	200	0.00151
200	1.5	1000	100	0.00201
500	1.5	1000	100	0.00201
200	2	1000	100	0.00201
500	2	1000	100	0.00201
200	1.5	2000	100	0.00201
500	1.5	2000	100	0.00201
200	2	2000	100	0.00201
500	2	2000	100	0.00201
200	1.5	1000	300	0.00201
500	1.5	1000	300	0.00201
200	2	1000	300	0.00201
500	2	1000	300	0.00201
200	1.5	2000	300	0.00201
500	1.5	2000	300	0.00201
200	2	2000	300	0.00201
500	2	2000	300	0.00201
200	1.75	1500	200	0.00201
500	1.75	1500	200	0.00201
350	1.5	1500	200	0.00201
350	2	1500	200	0.00201
350	1.75	1000	200	0.00201
350	1.75	2000	200	0.00201
350	1.75	1500	100	0.00201
350	1.75	1500	300	0.00201
350	1.75	1500	200	0.00201

These generated experimental points will be analyzed numerically. The pressure drop and thermal resistance outputs will be put in the MINITAB software to generate the second-order response equations.

3.4. Numerical Studies

Three-dimensional numerical simulations are performed in ANSYS Fluent. In order to perform the numerical studies, a numerical model is required to be set and validated. For this purpose, a suitable study from literature is found. After a working and validated model is obtained, the required numerical analyses are performed.

3.4.1. Validation of Numerical Model

Validation of the numerical model is accomplished with Lorenzini's experimental and numerical study [43]. They inspected the effect of variable pin fin clustering for non-uniform heat flux conditions. Firstly, the experiments are performed, and then they created a numerical model. Finally, they validated it with their own experimental data. They also created a reduced domain shown in Figure 3.5 for the researchers who are interested in variable pin fin effects. This reduced domain is used in the current study for validation before continuing with the CFD simulations of the T/R module heat sink.

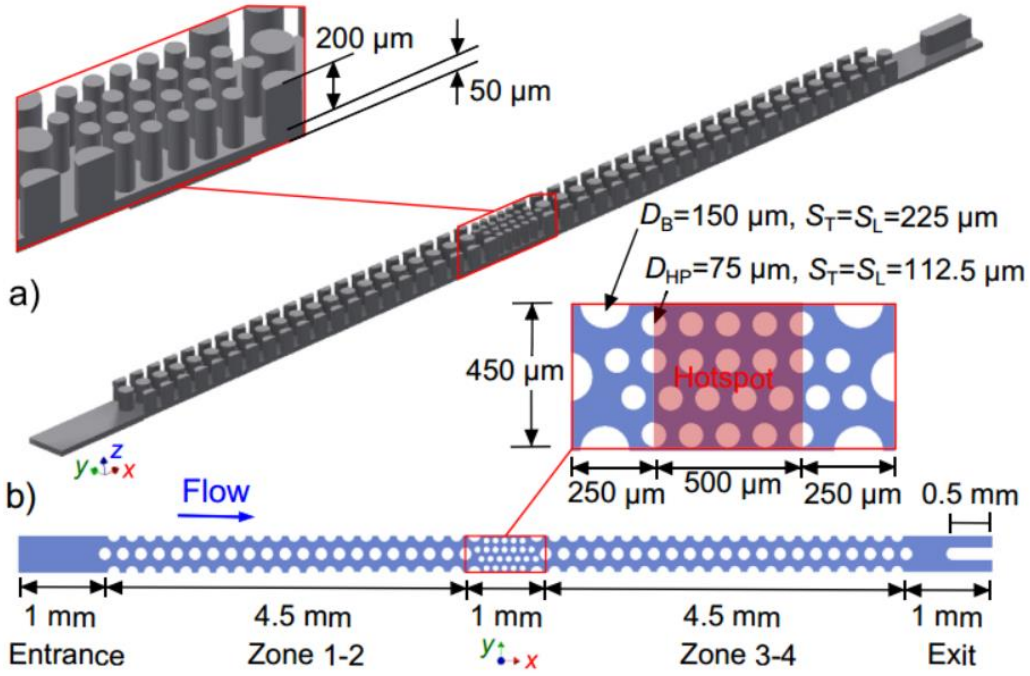

Figure 3.5. Geometric features and dimensions of the reduced domain [43]

Symmetry boundary conditions were assigned on both sides of the model, and high heat flux is applied at the hotspot region, and lower heat flux is applied to the bottom surface at Zone 1-2 and Zone 3-4 as seen in Figure 3.5.

Additionally, this case is a conjugate heat transfer model since the temperature variation along the solid domain is critical. The assumptions for the conjugate model and thermophysical properties are stated below:

- Flow is steady-state, laminar and incompressible.
- Radiation heat transfer effects are negligible.
- Temperature-dependent fluid and solid thermophysical properties are used.
- Viscous dissipation is negligible.

The coolant used in the model is water, and the solid domain is silicon, which is used at 3D stacked integrated circuits. The details of the properties used in the model are given in Table 3.3. Dynamic viscosity of the water is temperature-dependent, so water dynamic viscosity in the range 273 to 373 K is obtained with Equation (3.7) from [56]. Kandlikar et al. stated that there could be 30% pressure drop deviation because of the constant viscosity assumption. Another temperature dependent property, thermal conductivity of the silicon is retrieved from [24]. Conductivity values are curve fitted and expressed as a third-order polynomial. The remaining thermophysical properties such as specific heat, density of the fluid and solid domain are assumed constant since their variation is less than 5% for the operating temperature in the problem.

Table 3.3. Water and Silicon properties

Properties	**Water**	**Silicon**
Density [$\frac{kg}{m^3}$]	998	2330
Specific heat [$\frac{J}{kg.K}$]	4182	712
Viscosity [Pa. s]	Eq.(3.7)	-
Thermal conductivity [$\frac{W}{m.K}$]	0.6	Eq.(3.8)

The equations used for water viscosity is [56]:

$$\mu = 2.414 \times 10^{-5} \times (10^{\frac{247.8}{T-140}}) \tag{3.7}$$

The equation used for silicon thermal conductivity is [57]:

$$k_{si} = 2122.1 - 16.765\,T + 4.8183 \times 10^{-2}T^2 - 4.7442 \times 10^{-5}T^3 \tag{3.8}$$

3.4.1.1. Validation Model Geometry and Boundary Conditions

The geometry used for validation is a reduced domain, which is presented in Lorenzini's study [43]. They shared a simplified the geometry for researchers who are interested in the variable pin fin clustering approach. The physical domain has a 450 µm width, 12 mm length and 250 µm height as seen in Figure 3.5. There are two different fin regions depending on the varied heat flux conditions. At the background heat flux region, applied heat flux is 250 W/cm2 and, at the hotspot region which is in the middle region of the silicon heatsink, heat flux of 750 W/cm2 is applied. Cylindrical pin fins at the background area have 150 µm diameter and 225 µm transverse and longitudinal pitch whereas cylindrical pin fins at the hotspot region have 75 µm diameter and 112.5 µm transverse and longitudinal pitch. These regions are illustrated in Figure 3.6.

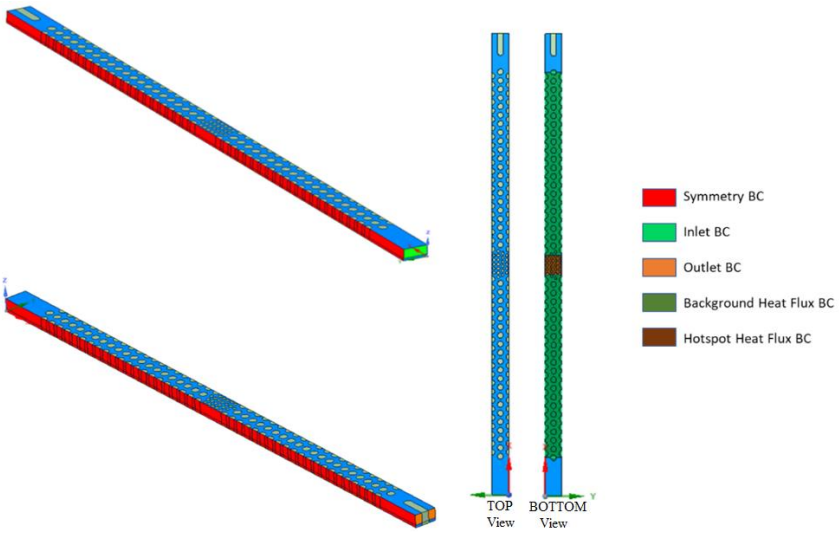

Figure 3.6. Boundary Conditions of Validation Model

The symmetry boundary condition is defined at each side of the domain. The inlet velocity of the water is given as 1.589 m/s which corresponds to 14.271×10^{-5} kg/s mass flow rate of water with an inlet temperature of 294.45 K. The outlet section is specified as a pressure outlet with zero-gauge pressure which makes the measurement of the pressure drop across the system possible. The remaining walls are assigned as adiabatic surfaces since heat losses are neglected.

A mesh independence study is applied. Flow is in the laminar range, but it has vortices because of the pin fins. The laminar model is used, and it is supported with boundary layer on fin surfaces. On the contrary to the general mesh approach in laminar flow, boundary layer is implemented into mesh to improve the convergence of the model. The Reynolds number in the inlet is calculated as 450. Convergence criteria are adjusted as 10^{-5} for continuity and 10^{-8} for energy residuals. In order to understand the presence of inflation layer, the mesh network is tried to be created without inflation layer, but it is seen that analysis doesn't converge with the absence of inflation. The sample mesh is given in Figure 3.7.

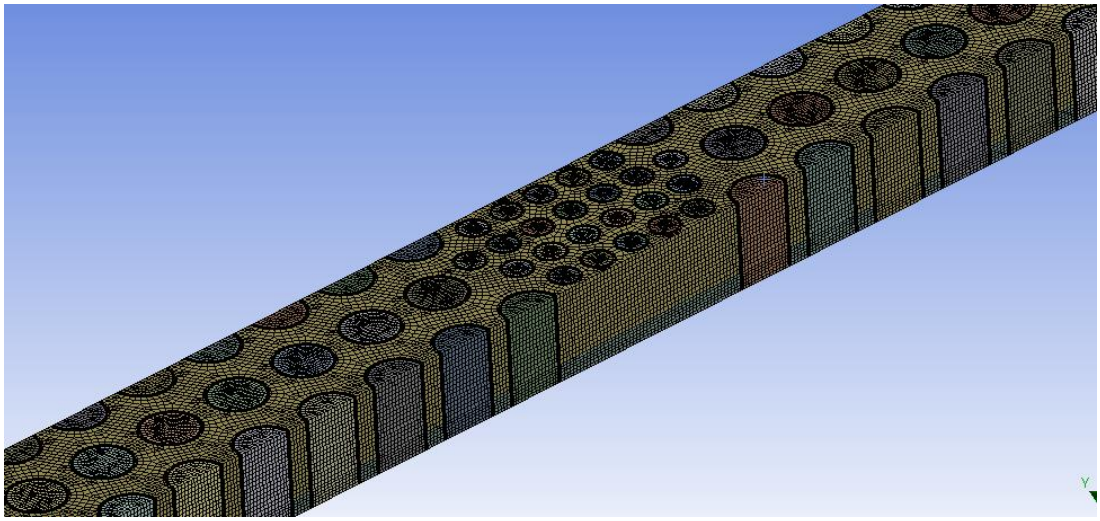

Figure 3.7. Created Mesh

The summary of the solver settings is given in Table 3.4.

Table 3.4. Solver Settings

Viscous Model	Laminar
Solution Controls	Pressure = 0.5
	Density = 1
	Body Forces = 1
	Momentum = 0.5
Discretization	Pressure = Second Order
	Momentum = Second Order Upwind
	Energy = Second Order Upwind
Pressure-Velocity Coupling	Coupled

The number of elements on the solid domain is not required to be high as in the fluid domain because the fluid domain is more critical due to the variable viscosity and conjugate heat transfer phenomena. The reference data for pressure drop and hotspot temperature are given as 137.28 kPa and 53.09 ºC, respectively. In Table 3.5; corresponding pressure drop and hotspot temperature results for each mesh setting is given. The mesh independence of the pressure and temperature can be also observed in Figure 3.8. The 4^{th} mesh configuration is found adequate. There is 7.7% error for pressure drop and 0.4% error for hotspot temperature in the model, compared with the experimental results in Lorenzini's study [43].

Table 3.5.Mesh independence of validation model

# of elements	Pressure drop [kPa]	Error [%]	Hotspot Temperature [ºC]	Error [%]
456000	198	-	52.9	-
660000	180	31	53	0.1
833000	141	2	53.1	0.01
1295000	**126.4**	**7.7**	**53.35**	**0.4**
1620000	125	8.7	53.45	0.6
2200000	126	8	53.47	0.7

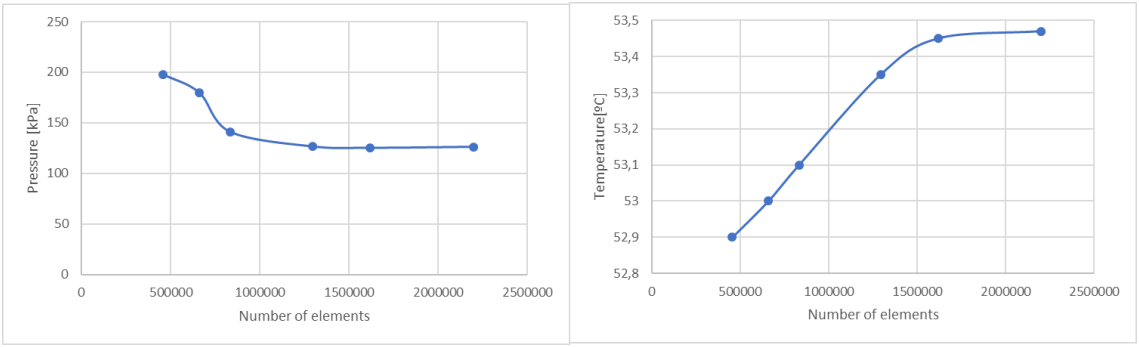

Figure 3.8. Mesh Independence Plot

For the validation of the model, six different mesh settings are used. Although the lowest error is obtained at the mesh setting, as the mesh is made finer, it is converged to larger value, so forth step settings are found adequate. With the given mesh settings, validation of the model is complete. These settings will be used for analyzing the temperature and pressure drop performance of non-uniform clustered pin-finned heat sink with non-uniform heat flux boundary conditions in the current thesis.

3.4.2. Mesh Configuration and Boundary Conditions of the Present Study

3.4.2.1. Boundary Conditions

In the numerical models, a constant mass flow rate of water is defined at the fluid inlet with an inlet temperature of 294.15 K. Due to the geometry of the flow channel, symmetry boundary condition is used to reduce the computational domain to half. The interface boundary condition is set automatically where the solid and fluid domain are in contact. The remaining walls, other than inlet, outlet, symmetry, and interface boundary condition, are considered as adiabatic. The hotspot and background heat fluxes are defined at the bottom of the solid domain. The related boundary conditions can be seen in Figure 3.9. In the figure, blue body is fluid domain and green body is solid domain.

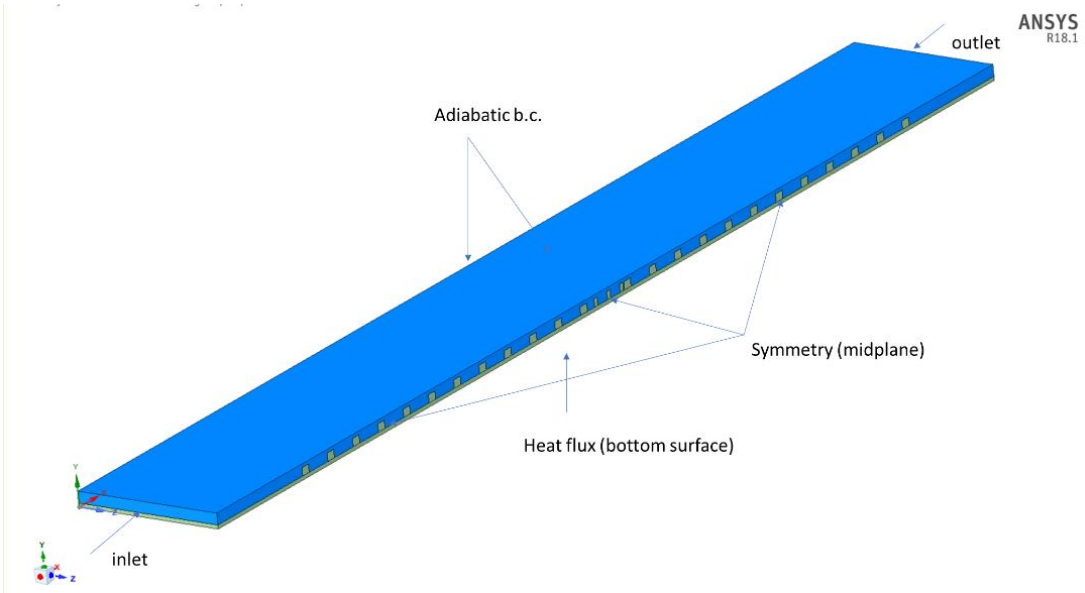

Figure 3.9. CFD Boundary Conditions

Boundary conditions can be expressed as equations. Heat flux at the bottom surface is;

$$-k_s \frac{\partial T}{\partial n}\Big|_{y=0} = q'' \tag{3.9}$$

where n is the surface normal vector. In the current study, the hotspot heat flux and background heat flux are 500 W/cm^2 and 200 W/cm^2, respectively.

At the inlet surface, predetermined mass flow rates are defined. It can be defined as;

$$\rho A u = C, at\ T = 294.15\ K \tag{3.10}$$

where C is the predetermined mass flow rate values, A is inlet area and ρ is density of water. The outlet boundary condition is defined as;

$$P_{out} = P_{atm} \tag{3.11}$$

At the solid-fluid interface boundary condition can be expressed as;

$$-k_s \frac{\partial T_s}{\partial n} = h\ (T_s - T_f) \tag{3.12}$$

where T_s is solid temperature, k_s is solid thermal conductivity, T_f is fluid temperature and h is heat transfer coefficient.

The side wall and upper wall are assumed as adiabatic surfaces. Therefore, the boundary condition at these surfaces is;

$$-k_s \frac{\partial T}{\partial n}\Big|_{y=0.4\ mm, z=0\ mm} = 0 \tag{3.13}$$

3.4.2.2. Meshing Studies

Once a working model is obtained, the validated mesh approach is applied to the present study. In order to be sure of using certain mesh settings, mesh independence study is repeated for present study's sample geometry since the scale of the current geometry is larger than the validation case.

When the previous mesh settings are used, the associated mesh consists of approximately 48 million mesh elements. Since using so many elements will cause a high computational cost, it is decided to repeat the mesh independence with the previous mesh approach for present geometry. Mesh independence is performed with an arbitrarily selected experiment point among the DOE set, which is heat sink with 350 μm diameter, 1.5 pitch ratio, 2000 μm hotspot fin array length, and 200 μm fin height. The results of the study are given in Table 3.6.

Table 3.6. Repeated mesh independence for current study scale

Mesh elements	Pressure Drop [kPa]	Relative Error [%]	Hotspot Temperature [K]	Relative Error [%]
7M	129.8	5.39	342.5	1.75
9M	135.2	1.45	346.2	0.69
22M	136.6	0.43	347.6	0.28
48M	137.2	-	348.6	-

As seen from the table, the 9 million setting can provide adequate results with reasonable error compared with the 48 million element mesh. The sample mesh is given in Figure 3.10 and Figure 3.11.

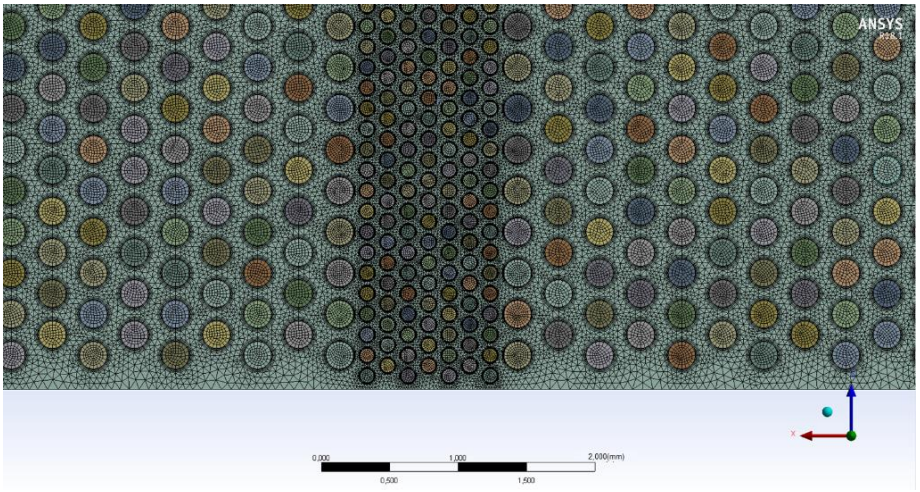

Figure 3.10. Sample mesh

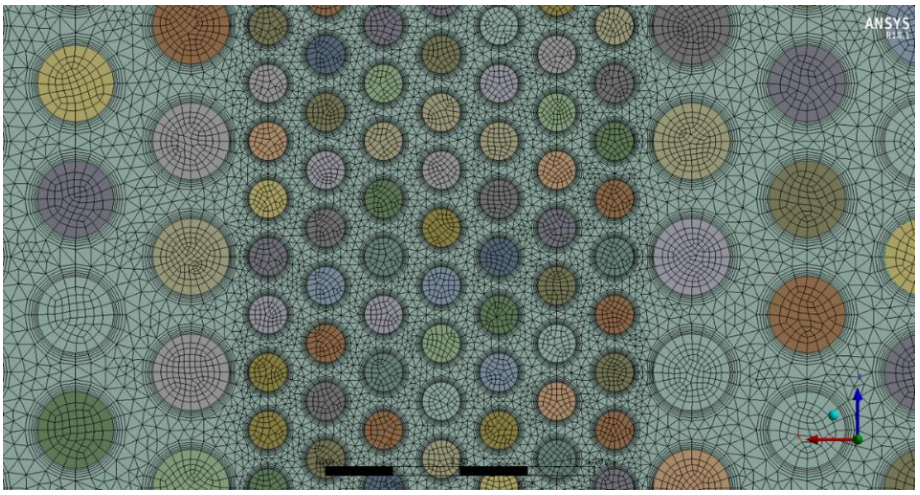

Figure 3.11. Mesh details

3.5. RSM

The purpose of creating a response surface function is obtaining precisely the replacement of the design objective functions in the defined design space. In this way, the optimum design solution will be acquired by optimizing the analytical models of

the thermal resistance and pressure drop. RSM is an acceptable way of obtaining the effect of all design variables on the response [35].

In this study, obtaining a response surface equation for the pressure drop, and thermal resistance is the objective to perform optimization study. The heat removal performance of heat sink is measured by thermal resistance [58]. In this work, the hotspot thermal resistance is determined as design objective, and it is defined as:

$$R_{th} = \frac{T_{hs} - T_{in}}{Q} \tag{3.14}$$

where T_{hs} is the average hotspot temperature, T_{in} is coolant inlet temperature, and Q is dissipated heat load [23,52,57]. Although the thermal resistance is defined from the hotspot region, the occurrence of higher background temperature is common since the hotspot heat load is a small portion of the total heat load [23]. By defining the thermal resistance as in Eq.(3.14), minimizing the hotspot temperature and maximizing the total heat removal are aimed simultaneously.

In numerical studies, pressure drop values are obtained by taking the difference of total pressure between the inlet and outlet of the heat sinks.

Q is the heat flow rate for the heat sink. It is calculated as:

$$Q = \dot{m}\, C_p\, \Delta T \tag{3.15}$$

where $\dot{m}$ is the mass flow rate of the coolant fluid, C_p is the specific heat, assumed as constant, and ΔT is the temperature difference ($\Delta T = T_{out} - T_{in}$) for the fluid. T_{in} is assumed constant for each case and T_{out} is changeable depending on the corresponding heat sink configuration. Corresponding outlet temperatures are obtained by mass-weighted average [60].

After the required results are obtained from the numerical analyses, Table 3.7 is prepared.

Table 3.7. DOE table with Results

Diameter (μm)	Pitch Ratio	HS Length (μm)	Fin Height (μm)	Mass flow rate [kg/s]	ΔP [Pa]	R_{th} [K/W]	Pumping Power [W]
200	1.5	1000	100	0.00101	7385.0	0.31527	0.0075
500	1.5	1000	100	0.00101	8176.0	0.19796	0.0083
200	2	1000	100	0.00101	7020.0	0.22374	0.0071
500	2	1000	100	0.00101	5196.0	0.22668	0.0053
200	1.5	2000	100	0.00101	5352.0	0.28233	0.0054
500	1.5	2000	100	0.00101	8010.0	0.19825	0.0081
200	2	2000	100	0.00101	7055.0	0.23904	0.0071
500	2	2000	100	0.00101	5164.0	0.23000	0.0052
200	1.5	1000	300	0.00101	134500.0	0.11690	0.1363
500	1.5	1000	300	0.00101	58460.0	0.14744	0.0592
200	2	1000	300	0.00101	52130.0	0.13381	0.0528
500	2	1000	300	0.00101	21070.0	0.17590	0.0213
200	1.5	2000	300	0.00101	141700.0	0.11501	0.1435
500	1.5	2000	300	0.00101	60360.0	0.13945	0.0611
200	2	2000	300	0.00101	55260.0	0.12761	0.0560
500	2	2000	300	0.00101	21070.0	0.17824	0.0213
200	1.75	1500	200	0.00101	30750.0	0.14102	0.0312
500	1.75	1500	200	0.00101	16900.0	0.16760	0.0171
350	1.5	1500	200	0.00101	32710.0	0.14736	0.0331
350	2	1500	200	0.00101	15330.0	0.17197	0.0155
350	1.75	1000	200	0.00101	23390.0	0.15473	0.0237
350	1.75	2000	200	0.00101	23550.0	0.15113	0.0239
350	1.75	1500	100	0.00101	7319.0	0.20444	0.0074
350	1.75	1500	300	0.00101	45060.0	0.14382	0.0456
350	1.75	1500	200	0.00101	23280.0	0.15296	0.0236
200	1.5	1000	100	0.00151	13670.0	0.22798	0.0207
500	1.5	1000	100	0.00151	16610.0	0.15551	0.0252
200	2	1000	100	0.00151	13540.0	0.16436	0.0205
500	2	1000	100	0.00151	10010.0	0.17723	0.0152
200	1.5	2000	100	0.00151	13790.0	0.24929	0.0209
500	1.5	2000	100	0.00151	16220.0	0.15385	0.0246
200	2	2000	100	0.00151	13610.0	0.17673	0.0206
500	2	2000	100	0.00151	9944.0	0.17882	0.0151
200	1.5	1000	300	0.00151	276200.0	0.08959	0.4183
500	1.5	1000	300	0.00151	122300.0	0.11279	0.1852
200	2	1000	300	0.00151	109100.0	0.10433	0.1652

Table 3.7. (Continued)

Diameter (μm)	Pitch Ratio	HS Length (μm)	Fin Height (μm)	Mass flow rate [kg/s]	ΔP [Pa]	Rth [K/W]	Pumping Power [W]
500	2	1000	300	0.00151	44280.0	0.13868	0.0671
200	1.5	2000	300	0.00151	290900.0	0.08767	0.4406
500	1.5	2000	300	0.00151	125900.0	0.11156	0.1907
200	2	2000	300	0.00151	115600.0	0.10172	0.1751
500	2	2000	300	0.00151	44210.0	0.13449	0.0670
200	1.75	1500	200	0.00151	61390.0	0.10752	0.0930
500	1.75	1500	200	0.00151	34620.0	0.13120	0.0524
350	1.5	1500	200	0.00151	65130.0	0.11417	0.0986
350	2	1500	200	0.00151	30760.0	0.13444	0.0466
350	1.75	1000	200	0.00151	46900.0	0.12303	0.0710
350	1.75	2000	200	0.00151	47320.0	0.11839	0.0717
350	1.75	1500	100	0.00151	14620.0	0.15736	0.0221
350	1.75	1500	300	0.00151	94010.0	0.11143	0.1424
350	1.75	1500	200	0.00151	46710.0	0.12177	0.0707
200	1.5	1000	100	0.00201	21340.0	0.18151	0.0430
500	1.5	1000	100	0.00201	27190.0	0.13122	0.0548
200	2	1000	100	0.00201	21740.0	0.13640	0.0438
500	2	1000	100	0.00201	16070.0	0.15309	0.0324
200	1.5	2000	100	0.00201	21410.0	0.20069	0.0432
500	1.5	2000	100	0.00201	26450.0	0.13092	0.0533
200	2	2000	100	0.00201	21860.0	0.14418	0.0441
500	2	2000	100	0.00201	15850.0	0.15432	0.0320
200	1.5	1000	300	0.00201	461700.0	0.07525	0.9308
500	1.5	1000	300	0.00201	205900.0	0.09510	0.4151
200	2	1000	300	0.00201	184900.0	0.09214	0.3728
500	2	1000	300	0.00201	74820.0	0.11361	0.1508
200	1.5	2000	300	0.00201	485700.0	0.07392	0.9792
500	1.5	2000	300	0.00201	212600.0	0.09331	0.4286
200	2	2000	300	0.00201	195700.0	0.08451	0.3945
500	2	2000	300	0.00201	74740.0	0.11411	0.1507
200	1.75	1500	200	0.00201	99740.0	0.08979	0.2011
500	1.75	1500	200	0.00201	56460.0	0.11311	0.1138
350	1.5	1500	200	0.00201	105400.0	0.09575	0.2125
350	2	1500	200	0.00201	50040.0	0.11606	0.1009
350	1.75	1000	200	0.00201	76560.0	0.10544	0.1543
350	1.75	2000	200	0.00201	77330.0	0.10086	0.1559
350	1.75	1500	100	0.00201	23820.0	0.13057	0.0480
350	1.75	1500	300	0.00201	159400.0	0.09546	0.3214

Table 3.7. (Continued)

Diameter (μm)	Pitch Ratio	HS Length (μm)	Fin Height (μm)	Mass flow rate [kg/s]	ΔP [Pa]	Rth [K/W]	Pumping Power [W]
350	1.75	1500	200	0.00201	77180.0	0.09915	0.1556

Table 3.7 is given as input to the MINITAB software to generate a second-order response surface equation for pressure drop and thermal resistance. Equation coefficients are given in Table A.1 and Table A.2.

The quadratic regression attempt has been performed, and it is seen that the regression function has significant errors in predictions, which will deteriorate the optimization study. The non-linearity of the pressure drop and thermal resistance results cause this outcome. In this case, Box-Cox transformation is a useful method to make the response variance closer to normal distribution [61]. In this method, response variables are subjected to power transformation.

Once the Box-Cox transformation applied, the quadratic response surface equations are generated. In Figure 3.12 and Figure 3.13, concurrency of the response equations is shown. The orange data represent the numerical solution results, and blue data represent the correlation results.

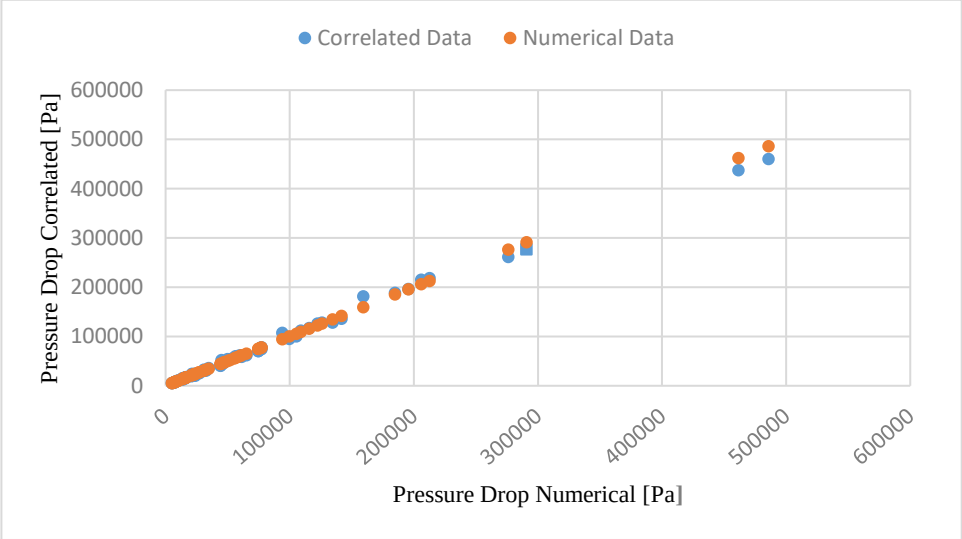

Figure 3.12. Pressure drop comparison plot

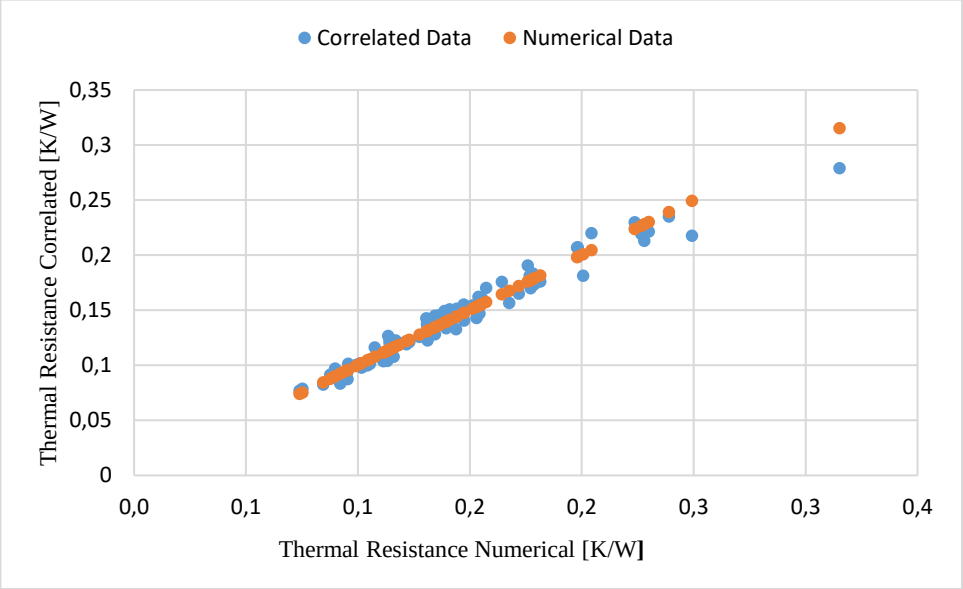

Figure 3.13. Thermal resistance comparison plot

Minitab provides a second-order response equation that has 99.70% average relative error with 99.59% adjusted R-square value for pressure drop and has 93.76% average relative error with 91.31% adjusted R-square value for thermal resistance. Because of

the complex geometric design of the pin fin and bypass effects [45], these values are acceptable. Adjusted R-square values are acceptable to use in the study.

3.5.1. Effect of the Design Variables

In order to analyze the design variables effect, the first step is calculation of the factor effect and t-value of the effect. The influence of one factor on the monitored response is calculated with the following equation

$$Effect = \frac{\sum_{i=1}^{n} y_i(+1) - \sum_{i=1}^{n} y_i(-1)}{n/2} \tag{3.16}$$

where y is the response for each point and n is the number of the experimental points at each level. Afterwards, t-value of the corresponding effect is obtained as

$$t - value_i = \frac{Effect_i}{\sqrt{MS_{residual}\left(\frac{1}{n(+1)} + \frac{1}{n(-1)}\right)}} \tag{3.17}$$

where $MS_{residual}$ is mean square of the residual calculated by Analysis of Variance and n is the number of responses from each studied level. Pareto plot of design variables' effect is drawn according to calculated t-values.

ANOVA is used for analyzing the experimental design which predicts the statistical significance of the factors on the response. There are some parameters used in the ANOVA analysis which are degrees of freedom, sums of squares, mean squares, F-value, P-value, mean square error, lack of fit, adjusted coefficient of determination and coefficient of determination. Statistical significance of the individual factors can be assessed from ANOVA table by considering F-value and P-values. The most significant effect on the response possesses P-value less than 0.05 and higher F-value. The calculation is this study are performed with α=0.05 significance level and 95% confidence interval which values are widely used in the literature. ANOVA tables of the current study are given in Table A.3 and Table A.4.

The Pareto chart is used as a graphical showing for the assessing the effects of the design variables and their interaction on the response functions which are thermal resistance and pressure drop. In the Pareto charts, main factors and their combinations are represented by bars, arranged in descending order according to the values of the standardized effects which is t-values. The vertical line stands for the statistical significance which depends on the significance level α. The main factors which cross the vertical line have statistical significance on the response [62].

The main factors are denoted with the A, B, C, D and E which are fin diameter, pitch ratio, hotspot fin array length, fin height and mass flow rate, respectively. The interaction terms shows the parameters' relation between each other. The quadratic terms (like DD) shows the quadratic behavior of the parameter. If a quadratic term is found out as statistically significant, it can be said that parameter shows quadratic behavior in specified design range [63].

3.5.1.1. Thermal Resistance

The standardized effects are summarized in Figure 3.14. In the figure, the standardized effects of design variables are shown from largest to smallest effect.

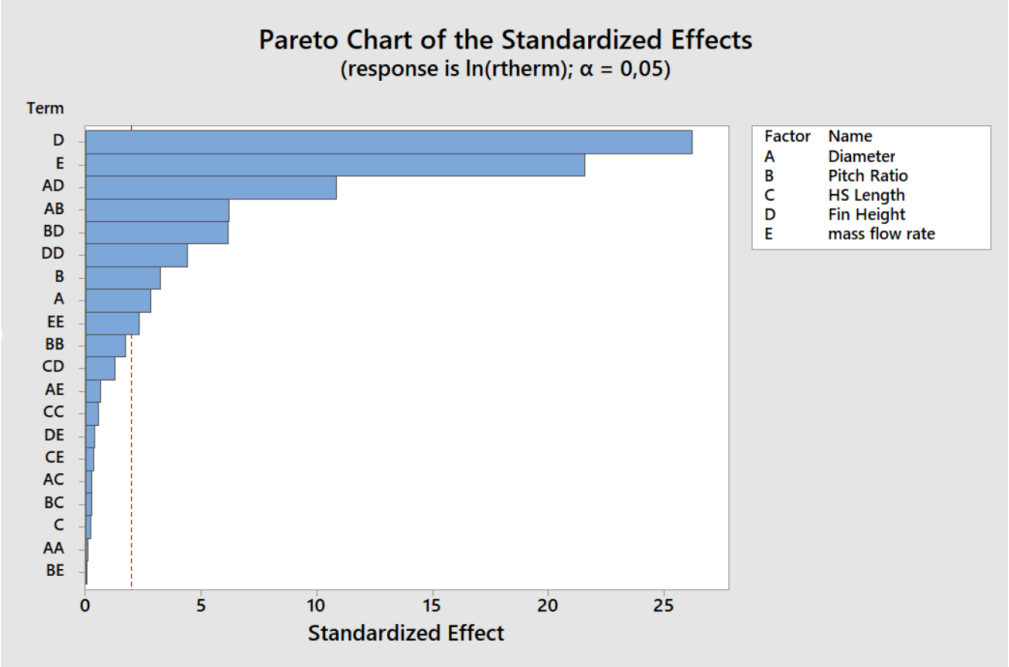

Figure 3.14. Design variables effect on Thermal Resistance

This figure implies that fin height has the most considerable effect on thermal resistance. It is seen that hotspot fin array length does not have considerable effect on the thermal resistance. The specified design variables in order from most significant to least significant influencer are; fin height, mass flow rate, pitch ratio, fin diameter, and hotspot fin array length. From Figure 3.14, influence of the interaction effects on the thermal resistance can be observed. In this aspect, fin diameter and fin height interaction have the most influence on the thermal resistance performance of the heat sink.

3.5.1.2. Pressure Drop

The design variable effect plot for the pressure is given in Figure 3.15.

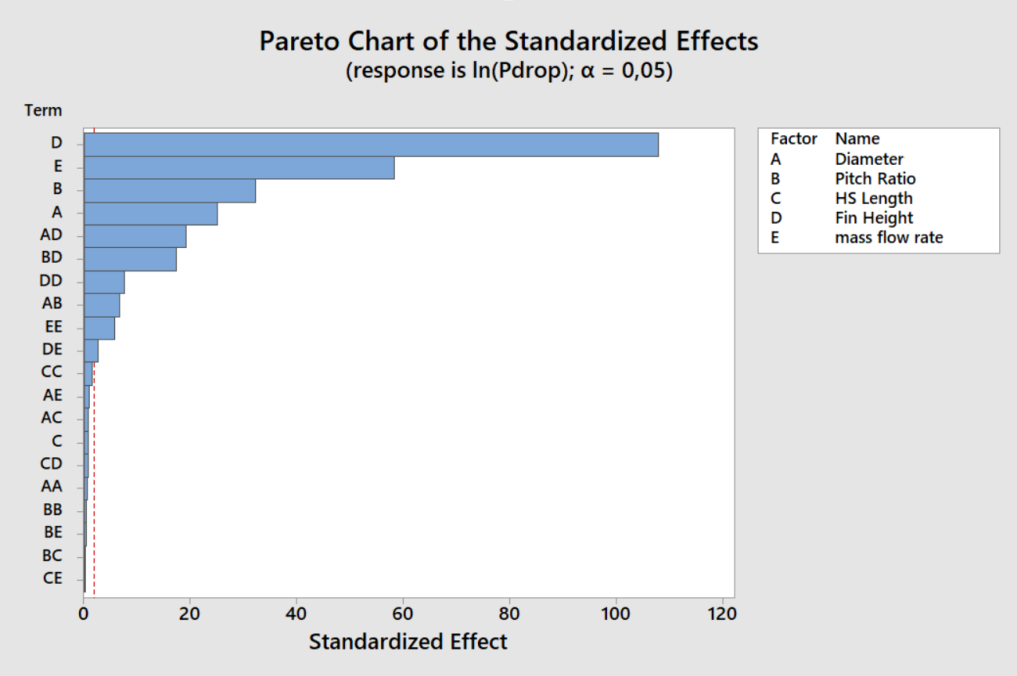

Figure 3.15. Design variables effect on Pressure Drop

For the pressure drop, fin height has the most considerable effect as in the thermal resistance performance. The list of the design variables from largest to smallest effect is as follows; fin height, mass flow rate, pitch ratio, fin diameter, and hotspot fin array length. In terms of interaction effects, fin diameter and fin height interaction have the most significant effect on the pressure drop performance statistically.

3.6. Optimization with Genetic Algorithm

It is complicated for designers to predict all the outcomes of changing design variables in a multi-variable problem because of the complicated relationship between design variables and responses. Design optimization techniques are very important at this stage.

MOGA is used as the optimization tool in this thesis. In multi-objective optimization method, the result is a set of optimal solutions. Enhancement in one objective causes

degradation of another one. Generally, this conflicting relationship can be observed within the Pareto front set. Depending on the system priorities, optimal design can be picked among the Pareto front set.

Considering the constraints in Table 3.8, MOGA is run, and the Pareto front (best solution set) is obtained for the specified objective functions. The temperature of the hotspot region is a critical objective to be fulfilled, which has a direct relation with the thermal resistance of the substrate. The maximum temperature limit is set as 363 K which is an acceptable upper limit for silicon devices [59]. Thus, minimizing the thermal resistance is determined as the first objective function. The second objective is minimizing the pressure drop across the pin finned heat sink since the structural limit for the silicon material enforces the pressure drop to be below 300 kPa [59]. As the flow rate or intensity of the pin fins increase, the two objectives show a conflicting behavior. While the pressure drop increases, thermal resistance exhibits a decreasing behavior. Therefore, the optimization is essential for determination of the optimum design point for fin diameter, fin height, fin pitch, and hotspot fin array length. In addition to hotspot temperature and pressure drop constraints, in order to have reasonable pumping power value, pumping power interval constraint is applied [32]. The Pareto front is shown in Figure 3.16. In the figure, distribution of the DOE analyses and Pareto front set can be observed.

The summary of the optimization process is given in Table 3.8.

Table 3.8. Optimization summary

Multi-Objective Functions	-Minimize Pressure drop -Minimize thermal resistance	
	Min. value	Max. value
Water mass flow rate	0.00101 kg/s	0.00203 kg/s
Fin height	100 µm	300 µm
Fin diameter	200 µm	500 µm
Pitch ratio	1.5	2
Hotspot fin array length	1000 µm	2000 µm
Module Power	403 W	
Constraints	Maximum hotspot temperature	363 K
	Maximum pressure drop	300 kPa
	Pumping Power	0.088-0.35W

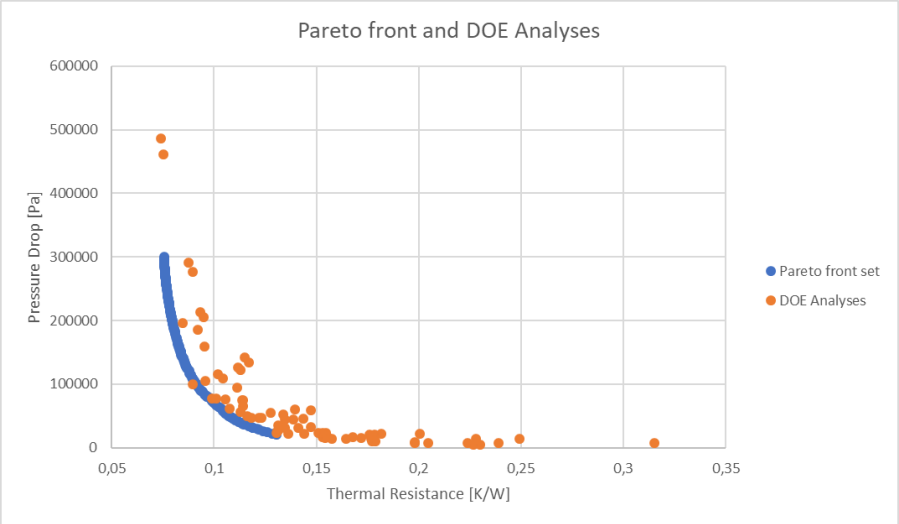

Figure 3.16. Pareto front set obtained by multi-objective genetic algorithm

The Pareto front set consists of 150 different design points. In multi-objective optimization problems, no solution in the Pareto front is better than the other solutions. The designer should choose a proper solution from the available solution set and

design constraints. It is seen that pumping powers ranged from 0.023 to 0.604 W. Considering the pumping power constraint in Table 3.8, preliminary elimination before the optimum solution selection is done. There are some methods called multi-objective decision-making methods to guide designer to choose best solution regarding the design strategy. TOPSIS (Technique for Order of Preference by Similarity to Ideal Solution), AHP (Analytic Hierarchy Process) are examples of the multi-objective decision-making methods.

TOPSIS is a classical and practical method for ranking and selecting alternatives. The choosing principle of the TOPSIS is finding the ideal point that should have the shortest distance from the positive ideal solution and the longest distance from the negative ideal solution. Because of these reasons, the TOPSIS method is found appropriate for choosing the best point process [64].

With the TOPSIS method, each objective is assigned weights according to their significance. In the current study, obtaining the lowest possible thermal resistance with an affordable pressure drop is the objective. Accordingly, thermal resistance has more priority than pressure drop. Therefore, weights are specified as;

$$W_1 + W_2 = 1 \tag{3.18}$$

where W_1 is thermal resistance weight, and W_2 is pressure drop weight.

In Figure 3.17, the red star represents the ideal best thermal resistance/ideal worst pressure drop design, and the green star represents the ideal best pressure drop/ideal worst thermal resistance design. There are three other stars in the figure, which represent the different weight factors' best solutions. The thermal resistance weights are 0.6, 0.5 and 0.4 and the corresponding pressure drop weights are 0.4, 0.5 and 0.6 for blue star, gray star and black star, respectively. In standard TOPSIS method applications, the weights are equal by default, but in this study, lower temperature values are desired for the module to be cooled, so lower thermal resistance is preferential. Therefore, weight of thermal resistance and pressure drop are preferred

as 0.6 and 0.4, respectively. The output of the current weights is found adequate for obtaining the low hotspot temperature while keeping pressure drop nominal.

With the determined weights, the performance ranking of the Pareto front is obtained as in Table 3.9.

Table 3.9. Performance Score Rating

Pin diameter [μm]	Pitch ratio	Hotspot fin array length [μm]	Pin height [μm]	Mass flow rate [kg/s]	Performance score
272.3	1.9475	1538.2	208.8	0.002	0.738271
245.3	1.9412	1511.4	210.6	0.002	0.737606
295.6	1.9226	1510.4	207.8	0.002	0.737282
217.3	1.9509	1512.1	208.9	0.002	0.737256
289.6	1.9462	1543.3	203.5	0.002	0.736366

According to the TOPSIS method, among the Pareto front set, the design solution with highest performance score is the best solution. In Table 3.9, among all, the first five design solutions with the highest performance score are given. These values are obtained with genetic algorithm, therefore after the optimum solution is selected, close values may be determined by rounding-off, considering the manufacturing techniques. In the current study, rounding-off is not applied in order to observe the consistency between the prediction and the CFD analysis result. The blue star design point is determined as the best design point with the TOPSIS decision making procedure. The selected point can be seen in the Pareto front plot in Figure 3.17.

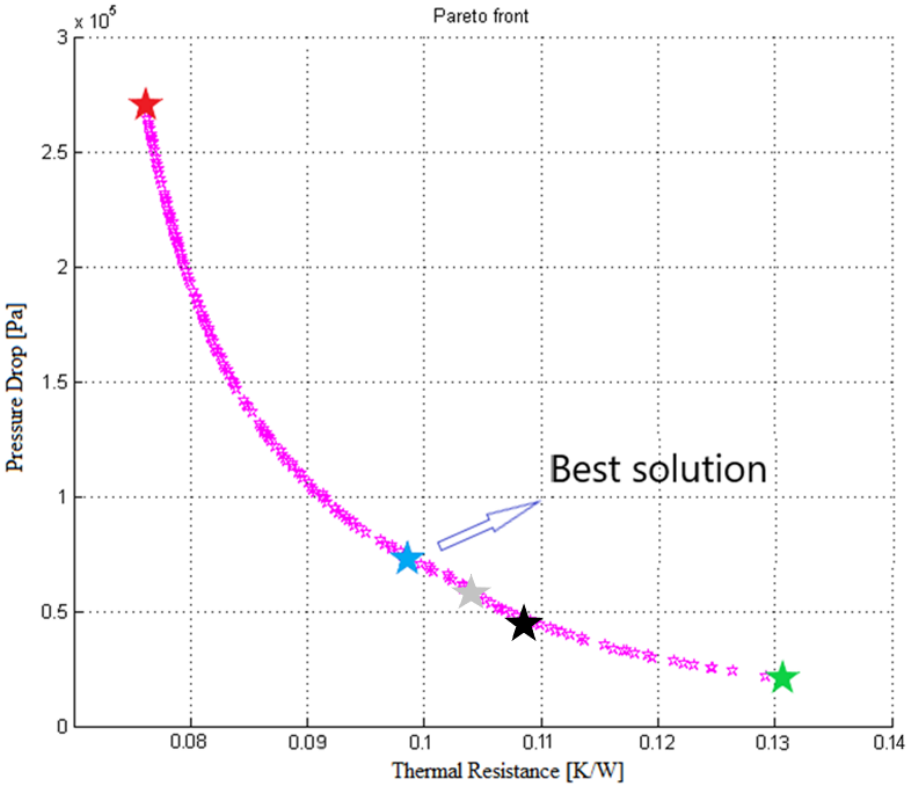

Figure 3.17. Illustration of the best solution within Pareto front set, Blue star W_1=0.6 W_2 =0.4, Gray star W_1=0.5 W_2 =0.5, Black Star W_1=0.4 W_2 =0.6

The best solution with the specified weights is provided in Table 3.10.

Table 3.10. Best solution determined by TOPSIS

Pin diameter [µm]	Pitch ratio	Hotspot fin array length [µm]	Pin height [µm]	Mass flow rate [kg/s]
272.3	1.947	1538	208.8	0.002

3.7. Comparison of Predicted Optimum Solution with CFD

In order to verify the validity of the quadratic models obtained with RSM, CFD confirmation analysis is performed to compare the thermal resistance and pressure drop predictions.

First, selected optimum design is drawn with the parameters in Table 3.10. The CAD model of the silicon part is illustrated in Figure 3.18. In the figure, the side walls are shown to better understand the geometry, but they are not included in the numerical solution domain since sidewalls and upper wall are assumed as adiabatic.

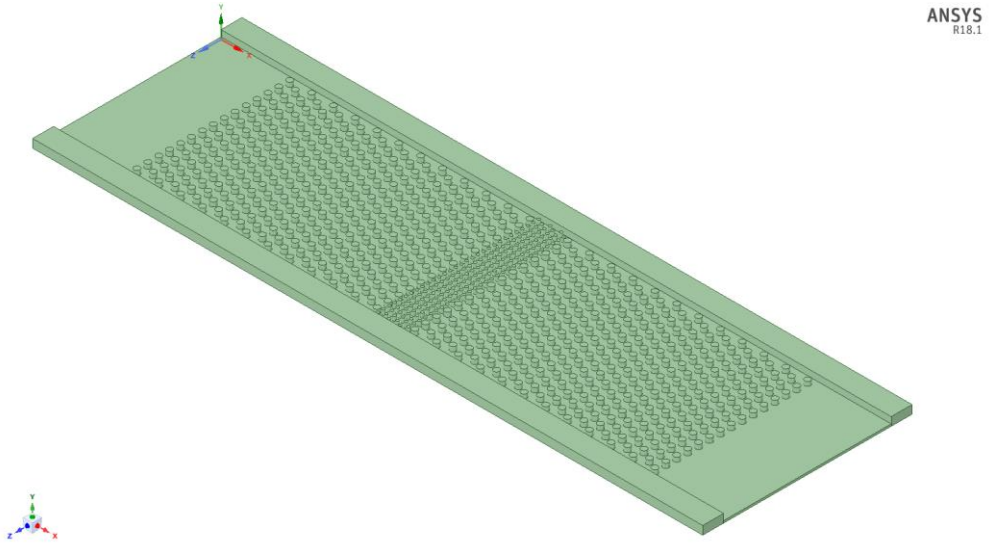

Figure 3.18. Selected optimum design

The same mesh approach in the DOE analysis is used for the optimum design. Consequently, the model of the optimum heat sink contains 8.95 million mesh elements. The solid and fluid domains of the mesh are given in Figure 3.19 and Figure 3.20, respectively.

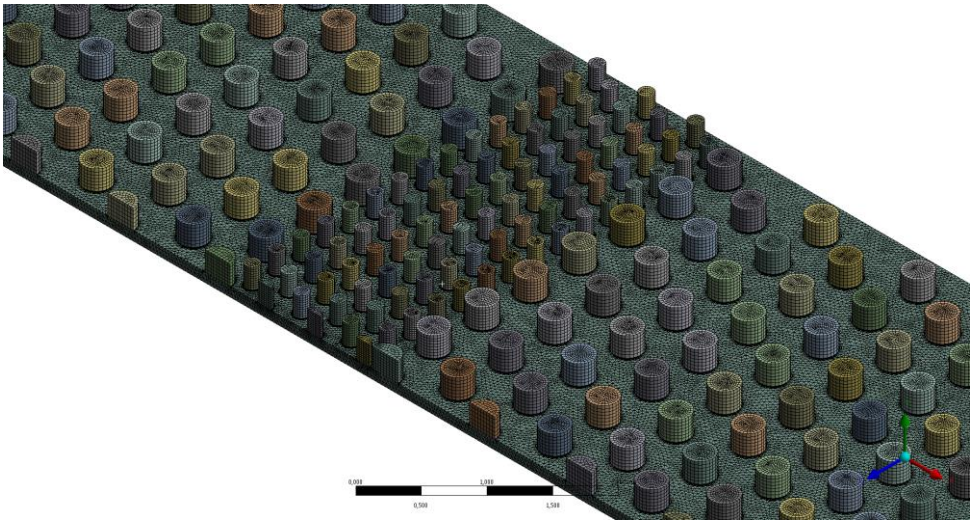

Figure 3.19. Solid Domain mesh

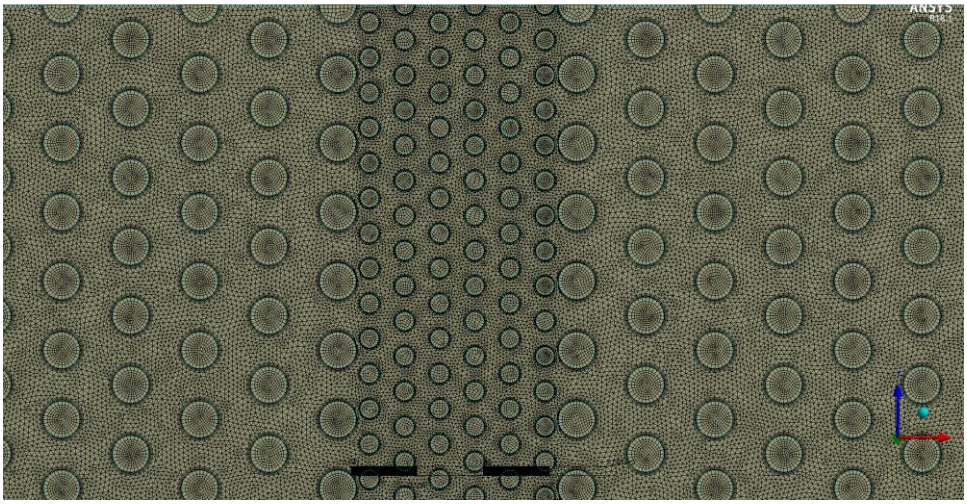

Figure 3.20. Fluid domain mesh

After the meshing is done, the next step is to do the CFD analysis. The solver settings in Table 3.4 are used. All simulations are done by using a high-performance computing (HPC) machine, which has an Intel Xeon CPU with 1000 physical cores. The analysis time is about 180 minutes.

The post-process outcomes of the optimum design are given in the Figures 3.21, 3.22 and 3.23.

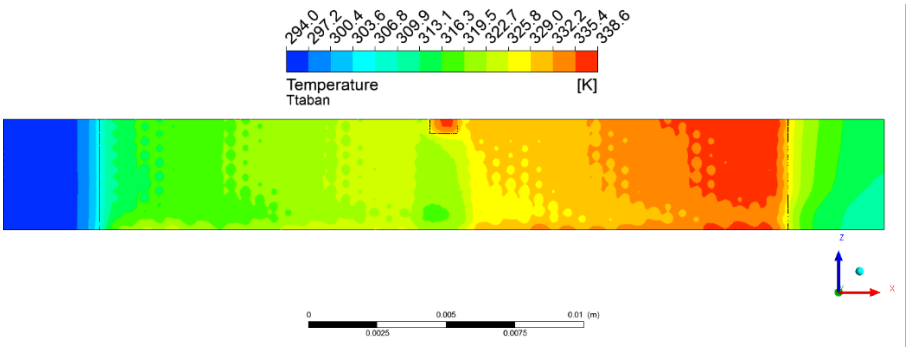

Figure 3.21. Temperature variation at heat sink base

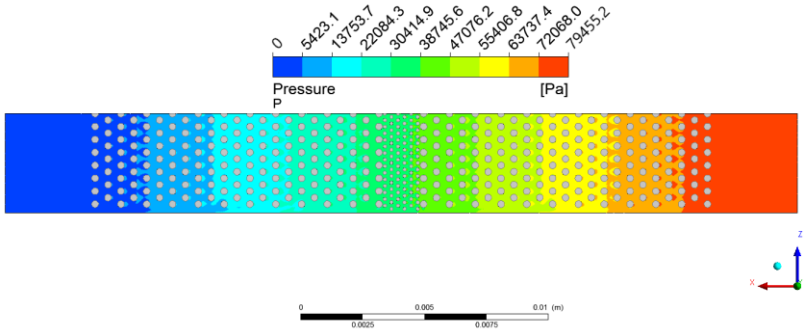

Figure 3.22. Water pressure variation at y = 0.25 mm

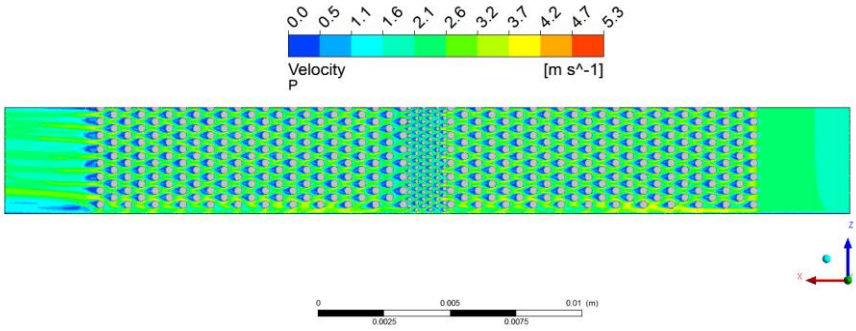

Figure 3.23. Water velocity variation at y = 0.25 mm

The comparison of the predicted and analyzed results are given in Table 3.11.

Table 3.11. Comparison Table

	Pressure Drop [Pa]	Thermal Resistance [K/W]
CFD Results	79455	0.09745
Response Surface Prediction	73466	0.0989
Error (%)	7.54	1.47

In the analysis of the optimized heat sink, it is seen that the maximum temperatures are measured as 336.7 K in the hotspot region and 338 K in the background region in Figure 3.27. This temperature is acceptable for the silicon device since it is lower than the tolerable steady-state working temperature 358 K [32]. The heat enhancement effect of the closely clustered small pin fins can be observed clearly at the densely finned background heat flux area. The increased heat transfer area causes this result. In Figure 3.21, the difference between the hotspot area and background can be observed easily. From pressure and velocity distribution figures, Figure 3.22 and Figure 3.23, it is seen that flow distribution along the pin fins is quite balanced which contributes to the good heat transfer. The flow is introduced into the channel uniformly; therefore, coolant flow increases when it flows through the pin fins. The velocity behind the fins is very low because of the pin blockage. Fluid flow behind fin can be observed in Figure 3.24. This blockage makes some coolant to do circulation motion at the pin fins' back area, which enhances the heat transfer [58]. Preventing the side bypass is crucial because it causes higher pressure drop compared to the top bypass [65]. Also, top bypass flow is directly related to the overall heat transfer. In order to observe the top bypass flow clearly, Figure 3.25 is obtained by filtering the flow speed 4 m/s and above with red color. In the figure, fluid domain velocity

distribution is given. As seen in the figure, the flow bypasses occur as top bypass at the dense pin fin array area and as side bypass close to the side wall. In order to observe the velocity contours further, Figure 3.26 is provided which shows the mid-section in z and y axes.

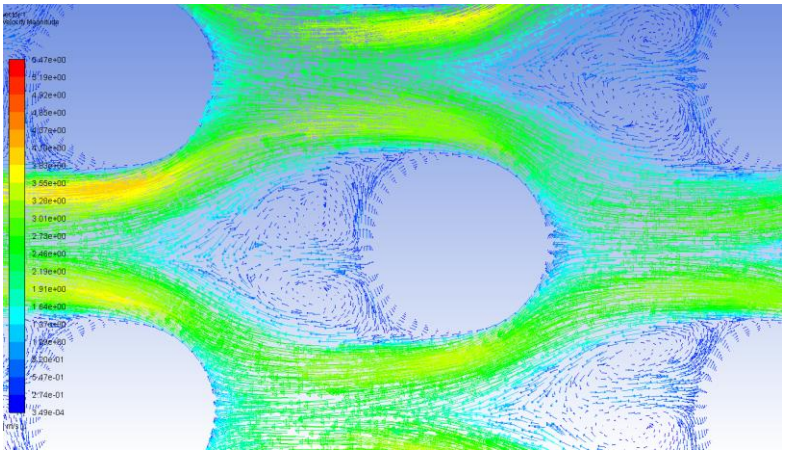

Figure 3.24. Fluid flow behind the pin fin

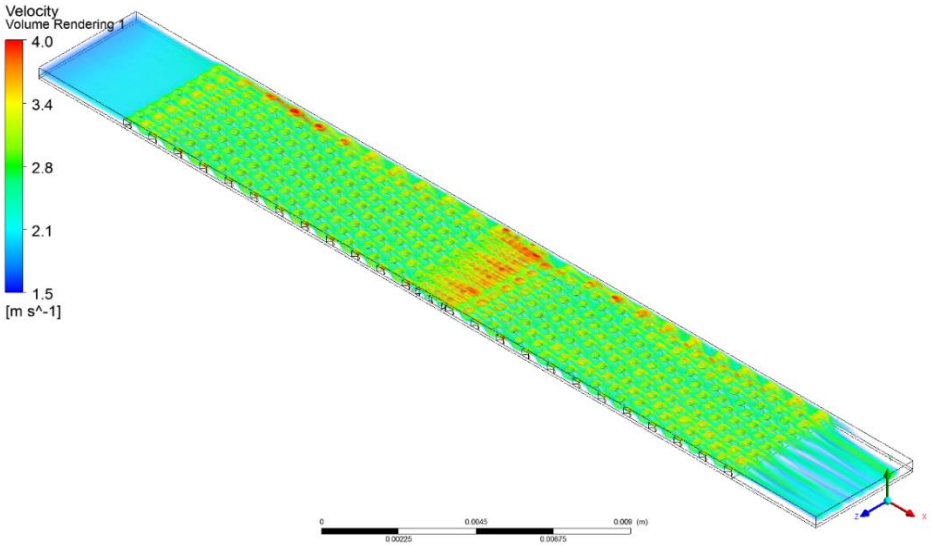

Figure 3.25. Bypass flows

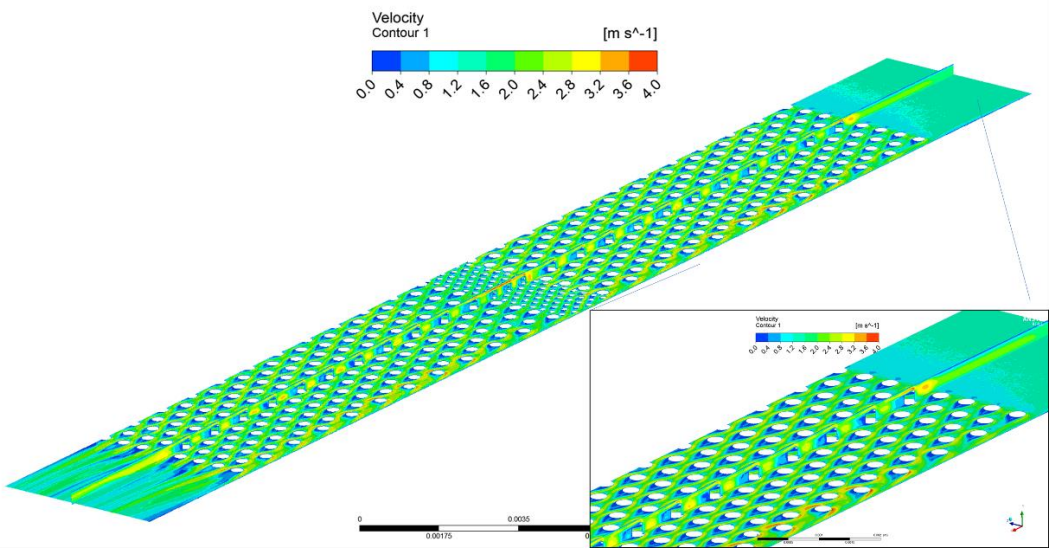

Figure 3.26. Velocity contours at mid-sections

The temperature variation at the hotspot region is given in Figure 3.27. It is seen that temperature variation is around the average temperature in most parts of the hotspot region. The use of the average temperature in the calculations seem reasonable for this study since temperature values are considerably lower than the critical temperatures.

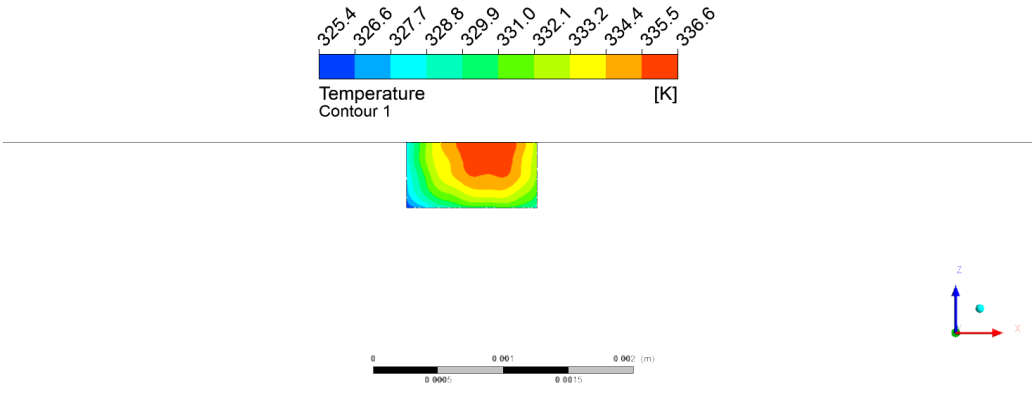

Figure 3.27. Hotspot region temperature variation

The thermal resistance value is quite consistent with the prediction. The error for the thermal resistance compared with the optimization prediction is found as 1.47%. However, the pressure drop is found as 79455 Pa, which corresponds to 7.54% error compared to the predicted result. There are two possible reasons for discrepancy between predictions and analyses. The first possible source of error is the side flow bypasses. The bypass flow deteriorates the hydraulic performance of the heat sink, so bypass flow causes pressure drop increase [65]. The velocity variation along the channel can be observed in Figure 3.23 and Figure 3.25. In the figure, it is seen that flow is equally distributed, but there are small bypass flows at the side and top of the heat sink, which affects the thermohydraulic performance. Secondly, the CFD errors in the DOE process augments the response surface equation regression error which will affect the predicted value. The implemented mesh settings may not be suitable for each case so the result may deviate. However, this methodology gives an idea about how each design variable affects the performance. The method can be divided into two sequential steps. In first step, the preferred design space can be scanned roughly, and according to desired solutions, design space can be minimized with the first solution set. The second cycle with minimized design space can be scanned in terms of DOE with increased resolution, and more accurate results can be obtained

CHAPTER 4

CONCLUSION

4.1. Summary of the Thesis Work

In this study, optimization of an embedded circular pin fin heat sink with non-uniform heat flux condition is performed with statistical methods, considering the increasing heat flux density in a transmitter/receiver module of a phase array radar application. The objective functions for guiding the optimization study are determined as thermal resistance and pressure drop along the heat sink. For this purpose, a few fin types are taken into consideration, but circular pin fin is preferred.

Heat sink CFD analyses are performed with half of the solution domain by taking advantage of the symmetry condition. The coolant fluid is considered as water, and the Reynolds number of the water is in the laminar range since microscale applications are expected to be in this regime [66]. Accordingly, mass flow rates are determined. Laminar flow viscous model is used since the validation of the model is done with Lorenzini's work [43].

For the defined heat sink geometry, design parameters are determined as fin diameter, pitch ratio, hotspot fin array length, fin height, and mass flow rate. In order to investigate the effect of these parameters on pressure drop and thermal resistance performance of the heat sink, and to do optimization study, statistical methods are employed. Design of experiments is used to create a design space within the specified upper and lower bounds of the investigated parameters. Response surface methodology is employed to correlate the relationship between design objectives and design variables. The non-linear behavior of the pressure drop, and thermal resistance causes error on regression analysis. In order to minimize the regression equation error, Box-Cox transformation is applied to the responses to make response variance closer

to the normal distribution. Once the transformed results are closer to normal variance, a more reliable regression analysis is performed. The genetic algorithm, which is a stochastic optimization method, is a good match for this problem to fulfill the search of all design domains for five design variables. By implementing the constraints and design space, multi-objective genetic algorithm is performed for pressure drop and thermal resistance of the heat sink. A Pareto front set is created, and with the help of TOPSIS method, an optimum design is selected. Finally, the comparison of the predicted result and the numerical result for the selected optimum design is made.

4.2. Conclusions

According to the analyses, it is found that fin height is the most important parameter for both thermal resistance and pressure drop performance of the heat sink. After the fin height, mass flow rate of the coolant fluid, pitch ratio and fin diameter have impact on thermal resistance and pressure drop, respectively. Additionally, through the RSM, the effects of interactions between the design parameters on the objective functions are observed in this study. Among the parameter interactions; fin diameter-fin height, fin diameter-pitch ratio, and pitch ratio-fin height interactions have influence on the thermal resistance performance. In terms of pressure drop, the sequence of the parameter interaction effect is fin diameter-fin height, pitch ratio-fin height, and fin diameter-pitch ratio.

After the optimization study, an optimum design is selected and modelled for 403 W heat load. The obtained thermal resistance value for the optimum solution is 0.09745 K/W, and corresponding pressure drop is 79455 Pa. The maximum temperature at the hotspot region is found as 336 K which is substantially below the maximum allowable silicon temperature [32].

The main contribution of the present study is that a design optimization methodology has been established for variable clustering of the pin fins in the presence of hotspot for a T/R module. While doing optimization, with the help of the RSM, the influence

of the inspected design variables on the thermal resistance and pressure drop performance is revealed.

4.3. Recommendations for Future Works

In this study, single-phase liquid-cooled heat sink is analyzed numerically and is optimized. There are a lot of assumptions made during the computational work. These assumptions can be improved to model a more realistic case. Primarily, all fluid and solid properties can be modeled temperature dependent rather than the only fluid viscosity and solid thermal conductivity. Additionally, a more automatized geometry generation and mesh creating structure may be constructed. In this way, as the DOE setup is ready, geometry generation, meshing, and CFD analyzing can be made efficient in time.

The DOE method is set up with 75 experiment points, which is the minimum number to scan the design space, so additional experiment points may be defined and performed to obtain better representation of the problem.

Finally, an experimental study can be performed in order to compare the numerical results.

REFERENCES

[1] R. Ashford and S. Brown, “F-22 Environmental Control System/Thermal Management System (ECS/TMS) Flight Test Program - Downloadable Constants, an Innovative Approach,” 2000.

[2] U.S. Department of Defense, “Reliability prediction of electronic equipment,” Springfield, 1974.

[3] T. Van Oevelen, *Optimal Heat Sink Design for Liquid Cooling of Electronics*, no. November. 2014.

[4] D. B. Tuckerman and R. F. W. Pease, “High-performance heat sinking for VLSI,” *IEEE Electron Device Lett.*, vol. 2, no. 5, pp. 126–129, 1981.

[5] V. Lakshminarayanan and N. Sriraam, “The effect of temperature on the reliability of electronic components,” *IEEE CONECCT 2014 - 2014 IEEE Int. Conf. Electron. Comput. Commun. Technol.*, pp. 1–6, 2014.

[6] C. Bailey, “Thermal management technologies for electronic packaging: Current capabilities and future challenges for modelling tools,” *10th Electron. Packag. Technol. Conf. EPTC 2008*, pp. 527–532, 2008.

[7] R. Mahajan, C. P. Chiu, and G. Chrysler, “Cooling a microprocessor chip,” *Proc. IEEE*, vol. 94, no. 8, pp. 1476–1485, 2006.

[8] G. E. Moore, “Cramming more components onto integrated circuits, Reprinted from Electronics, volume 38, number 8, April 19, 1965, pp.114 ff.,” *IEEE Solid-State Circuits Soc. Newsl.*, vol. 11, no. 3, pp. 33–35, Sep. 2006.

[9] A. Scott, *Cooling of electronic equipment*. New York: John Wiley and Sons, 1974.

[10] S. M. Sohel Murshed and C. A. Nieto de Castro, “A critical review of traditional and emerging techniques and fluids for electronics cooling,” *Renew. Sustain. Energy Rev.*, vol. 78, no. March 2016, pp. 821–833, 2017.

[11] J. F. Tullius, R. Vajtai, and Y. Bayazitoglu, “A review of cooling in microchannels,” *Heat Transf. Eng.*, vol. 32, no. 7–8, pp. 527–541, 2011.

[12] S. G. Kandlikar and W. J. Grande, “Evolution of microchannel flow passages-thermohydraulic performance and fabrication technology,” *Heat Transf. Eng.*, vol. 24, no. 1, pp. 3–17, 2003.

[13] A. Sadeghi, A. Asgarshamsi, and M. H. Saidi, “Laminar Forced Convection in Annular Microchannels With Slip Flow Regime,” in *ASME 2009 7th International Conference on Nanochannels, Microchannels and Minichannels*,

2009, pp. 353–361.

[14] C. Nonino, S. Del Giudice, and S. Savino, “Temperature-Dependent Viscosity and Viscous Dissipation Effects in Microchannel Flows With Uniform Wall Heat Flux,” *Heat Transf. Eng.*, vol. 31, no. 8, pp. 682–691, Jul. 2010.

[15] H. Shokouhmand, M. Aghvami, and M. J. Afshin, “Pressure Drop and Heat Transfer of Fully Developed, Laminar Flow in Rough, Rectangular Microchannels,” in *ASME 2008 6th International Conference on Nanochannels, Microchannels, and Minichannels*, 2008, pp. 153–157.

[16] S. A. Solovitz, “Computational Study of Grooved Microchannel Enhancements,” in *ASME 2008 6th International Conference on Nanochannels, Microchannels, and Minichannels*, 2008, pp. 1407–1414.

[17] N. Baghernezhad and O. Abouali, “Numerical Investigation of Single Phase Heat Transfer Enhancement in a Microchannel With Grooved Surfaces,” in *ASME 2008 6th International Conference on Nanochannels, Microchannels, and Minichannels*, 2008, pp. 233–240.

[18] S. Vanapalli *et al.*, “Pressure drop of laminar gas flows in a microchannel containing various pillar matrices,” *J. Micromechanics Microengineering*, vol. 17, no. 7, pp. 1381–1386, Jul. 2007.

[19] Y.-J. Lee, P.-S. Lee, and S.-K. Chou, “Enhanced Microchannel Heat Sinks Using Oblique Fins,” in *ASME 2009 InterPACK Conference, Volume 2*, 2009, pp. 253–260.

[20] X. Zhong, Y. Fan, J. Liu, Y. Zhang, T. Wang, and Z. Cheng, “A study of CFD simulation for on-chip cooling with 2D CNT micro-fin array,” *Proc. Int. Symp. High Density Packag. Microsyst. Integr. 2007, HDP’07*, no. 149, pp. 3–8, 2007.

[21] T. Brunschwiler, A. Sridhar, C. L. Ong, and G. Schlottig, “Benchmarking study on the thermal management landscape for three-dimensional integrated circuits: From back-side to volumetric heat removal,” *J. Electron. Packag. Trans. ASME*, vol. 138, no. 1, 2016.

[22] C. A. Rubio-Jimenez, S. G. Kandlikar, and A. Hernandez-Guerrero, “Numerical analysis of novel micro pin fin heat sink with variable fin density,” *IEEE Trans. Components, Packag. Manuf. Technol.*, vol. 2, no. 5, pp. 825–833, 2012.

[23] T. E. Sarvey *et al.*, “Integrated Circuit Cooling Using Heterogeneous Micropin-Fin Arrays for Nonuniform Power Maps,” *IEEE Trans. Components, Packag. Manuf. Technol.*, vol. 7, no. 9, pp. 1465–1475, 2017.

[24] D. Lorenzini-Gutierrez and S. G. Kandlikar, “Variable Fin Density Flow Channels for Effective Cooling and Mitigation of Temperature Nonuniformity in Three-Dimensional Integrated Circuits,” *J. Electron. Packag.*, vol. 136, no.

2, p. 021007, 2014.

[25] J. Li and G. P. Peterson, "3-Dimensional numerical optimization of silicon-based high performance parallel microchannel heat sink with liquid flow," *Int. J. Heat Mass Transf.*, vol. 50, no. 15–16, pp. 2895–2904, 2007.

[26] W. A. Khan, J. R. Culham, and M. M. Yovanovich, "Optimization of Microchannel Heat Sinks Using Entropy Generation Minimization Method," *IEEE Trans. Components Packag. Technol.*, vol. 32, no. 2, pp. 243–251, Jun. 2009.

[27] G. Hu and S. Xu, "Optimization design of microchannel heat sink based on SQP method and numerical simulation," in *2009 International Conference on Applied Superconductivity and Electromagnetic Devices*, 2009, pp. 89–92.

[28] A. M. Adham, N. Mohd-Ghazali, and R. Ahmad, "Optimization of an ammonia-cooled rectangular microchannel heat sink using multi-objective non-dominated sorting genetic algorithm (NSGA2)," *Heat Mass Transf.*, vol. 48, no. 10, pp. 1723–1733, Oct. 2012.

[29] Y. O. Abdelsalam, S. Alimohammadi, Q. Pelletier, and T. Persoons, "A multi-objective genetic algorithm optimisation of plate-fin heatsinks," *THERMINIC 2017 - 23rd Int. Work. Therm. Investig. ICs Syst.*, vol. 2017-Janua, no. September, pp. 1–6, 2017.

[30] T. Andersson, D. Nowak, T. Johnson, A. Mark, F. Edelvik, and K. H. Küfer, "Multiobjective Optimization of a Heat-Sink Design Using the Sandwiching Algorithm and an Immersed Boundary Conjugate Heat Transfer Solver," *J. Heat Transfer*, vol. 140, no. 10, 2018.

[31] G. Türkakar, "Numerical simulation and analytical optimization of microchannel heat sinks," METU, MS Thesis, 2010.

[32] G. Türkakar and T. Okutucu-Özyurt, "Dimensional optimization of microchannel heat sinks with multiple heat sources," *Int. J. Therm. Sci.*, vol. 62, pp. 85–92, 2012.

[33] T. D. Robinson, M. S. Eldred, K. E. Willcox, and R. Haimes, "Surrogate-based optimization using multifidelity models with variable parameterization and corrected space mapping," *AIAA J.*, vol. 46, no. 11, pp. 2814–2822, 2008.

[34] M. J. Asher, B. F. W. Croke, A. J. Jakeman, and L. J. M. Peeters, "A review of surrogate models and their application to groundwater modeling," *Water Resour. Res.*, vol. 51, no. 8, pp. 5957–5973, Aug. 2015.

[35] C. H.Myers, R., C.Montgomery, D., & Anderson-Cook, M, Response Surface Methodology: Process and Product Optimization Using Designed Experiments (Third Edition). WILEY SERIES IN PROBABILITY AND STATISTICS, 2016.

[36] M. Cavazzuti, *Optimization Methods: From Theory to Design: Design of Experiments*, no. September. 2003.

[37] R. Gheshlaghi, J. M. Scharer, M. Moo-Young, and P. L. Douglas, "Application of statistical design for the optimization of amino acid separation by reverse-phase HPLC," *Anal. Biochem.*, vol. 383, no. 1, pp. 93–102, 2008.

[38] K. Kant, S. Singh, and P. Dhiman, "Fluid flow and heat transfer characteristics within a rectangular microchannel array of different manifold shapes - modelisation and optimisation using CFD and response surface methodology," *Prog. Comput. Fluid Dyn. An Int. J.*, vol. 18, no. 1, p. 19, 2018.

[39] K. T. Chiang and F. P. Chang, "Application of response surface methodology in the parametric optimization of a pin-fin type heat sink," *Int. Commun. Heat Mass Transf.*, vol. 33, no. 7, pp. 836–845, 2006.

[40] Y.-J. Lee, P.-S. Lee, and S.-K. Chou, "Hot Spot Mitigating With Oblique Finned Microchannel Heat Sink," pp. 167–174, 2012.

[41] Y. Sui, C. J. Teo, P. S. Lee, Y. T. Chew, and C. Shu, "Fluid flow and heat transfer in wavy microchannels," *Int. J. Heat Mass Transf.*, vol. 53, no. 13–14, pp. 2760–2772, Jun. 2010.

[42] A. Koşar and Y. Peles, "TCPT-2006-096.R2: Micro scale pin fin heat sinks - Parametric performance evaluation study," *IEEE Trans. Components Packag. Technol.*, vol. 30, no. 4, pp. 855–865, 2007.

[43] D. Lorenzini *et al.*, "Embedded single phase microfluidic thermal management for non-uniform heating and hotspots using microgaps with variable pin fin clustering," *Int. J. Heat Mass Transf.*, vol. 103, pp. 1359–1370, 2016.

[44] "A review of ' Introduction to Heat Transfer ' Third Edition Frank P. Incropera & David P. de Witt, 1996 New York, Wiley ISBN 0471304581 £19.99," *Eur. J. Eng. Educ.*, vol. 21, no. 4, pp. 447–447, Dec. 1996.

[45] H. T. Chen, P. L. Chen, J. T. Horng, and Y. H. Hung, "Design optimization for pin-fin heat sinks," *J. Electron. Packag. Trans. ASME*, vol. 127, no. 4, pp. 397–406, 2005.

[46] M. J. Anderson and P. J. Whitcomb, *DOE Simplified*. New York: Productivity Press, 2017.

[47] I. K. Karathanassis, E. Papanicolaou, V. Belessiotis, and G. C. Bergeles, "Multi-objective design optimization of a micro heat sink for Concentrating Photovoltaic/Thermal (CPVT) systems using a genetic algorithm," *Appl. Therm. Eng.*, vol. 59, no. 1, pp. 733–744, 2013.

[48] D. L. Vrable and B. D. Donovan, "High heat flux thermal management for hpm sources," *SAE Tech. Pap.*, vol. 113, no. 2004, pp. 1958–1964, 2004.

[49] U. K. Revankar, K. Sreenivasulu, K. M. Veerabhadra, K. S. Beenamole, and D. Kumar, “An experimantal active aperture array for l-band high power active phased array radar,” in *IEEE International Symposium on Phased Array Systems and Technology, 2003.*, pp. 289–294.

[50] E. Alpsan, “Experimental Investigation And Numerical Analysis Of Microchannel Heatsinks For Phased Array Radar Cooling Applications,” Middle East Technical University, MS Thesis, 2008.

[51] B. E. Short, P. E. Raad, and D. C. Price, “Performance of pin fin cast aluminum coldwalls, Part 1: Friction factor correlations,” *J. Thermophys. Heat Transf.*, vol. 16, no. 3, pp. 389–396, 2002.

[52] W. A. Khan, J. R. Culham, and M. M. Yovanovich, “Convection heat transfer from tube banks in crossflow: Analytical approach,” *Int. J. Heat Mass Transf.*, vol. 49, no. 25–26, pp. 4831–4838, 2006.

[53] R. S. Prasher *et al.*, “Nusselt number and friction factor of staggered arrays of low aspect ratio micropin-fins under cross flow for water as fluid,” *J. Heat Transfer*, vol. 129, no. 2, pp. 141–153, 2007.

[54] F. Wang, J. Zhang, and S. Wang, “Investigation on flow and heat transfer characteristics in rectangular channel with drop-shaped pin fins,” *Propuls. Power Res.*, vol. 1, no. 1, pp. 64–70, 2012.

[55] W. Qu and I. Mudawar, “Experimental and numerical study of pressure drop and heat transfer in a single-phase micro-channel heat sink,” *Int. J. Heat Mass Transf.*, vol. 45, no. 12, pp. 2549–2565, 2002.

[56] T.Al-Shemmeri, *Engineering Fluid Mechanics*. Holland: Ventus Pubishinh, 2012.

[57] F-Chart Software,“Engineering Equation Solver.” .

[58] D. Yang, Y. Wang, G. Ding, Z. Jin, J. Zhao, and G. Wang, “Numerical and experimental analysis of cooling performance of single-phase array microchannel heat sinks with different pin-fin configurations,” *Appl. Therm. Eng.*, vol. 112, pp. 1547–1556, 2017.

[59] X. Zhang and Y. Jaluria, “Optimization of microchannel-based cooling systems,” *Numer. Heat Transf. Part A Appl.*, vol. 74, no. 3, pp. 1053–1067, 2018.

[60] Pathscale Corporation, *Ansys fluent 12.0*. 2009.

[61] M. H. Kutner, *Applied linear statistical models*, 4th ed. New York: The McGraw-Hill Company, 2004.

[62] A. Aleksiev, B. Kostova, and D. Rachev, “Development and optimization of the reservoirtype oral multiparticulate drug delivery systems of galantamine

hydrobromide," *Indian J. Pharm. Sci.*, vol. 78, no. 3, pp. 368–376, 2016.

[63] J. A. Stimson, E. G. Carmines, and R. A. Zeller, "Interpreting polynomial regression," *Sociol. Methods Res.*, vol. 6, no. 4, pp. 515–524, 1978.

[64] Y. Ge, Z. Liu, F. Shan, F. Yuan, R. Long, and W. Liu, "Multi-objective arrangement optimization of a tube bundle in cross-flow using CFD and genetic algorithm," *Energy Procedia*, vol. 142, pp. 3774–3779, 2017.

[65] N. Lei and A. Ortega, "Experimental hydraulic characterization of pin fin heat sinks with top and side bypass," *Thermomechanical Phenom. Electron. Syst. - Proceedings Intersoc. Conf.*, vol. 1, pp. 418–428, 2004.

[66] Y. Peles, A. Koşar, C. Mishra, C. J. Kuo, and B. Schneider, "Forced convective heat transfer across a pin fin micro heat sink," *Int. J. Heat Mass Transf.*, vol. 48, no. 17, pp. 3615–3627, 2005.

APPENDICES

A. APPENDIX

Table A.1. Correlation Coefficients for Natural logarithm of Pressure drop

Term	*Coefficient*
Constant	3.49
(A)Diameter	3.78
(B)Pitch ratio	1.39
(C)Hotspot fin array length	-0.424
(D)Fin height	34.60
(E)Mass flow rate	2165
A*A	0.72
B*B	-0.167
C*C	0.166
D*D	-19.78
E*E	-400720
A*B	-1.884
A*C	-0.124
A*D	-13.377
A*E	159
B*C	-0.0186
B*D	-7.225
B*E	37
C*D	0.169
C*E	-10.5
D*E	656

Table A.2. Correlation Coefficients for Natural logarithm of Thermal Resistance

Term	*Coefficient*
Constant	4.97
(A)Diameter	-4.367
(B)Pitch ratio	-3.41
(C)Hotspot fin array length	-0.167
(D)Fin height	-13.51
(E)Mass flow rate	-991
A*A	0.11
B*B	0.69
C*C	0.0547
D*D	10.92
E*E	157824
A*B	1.667
A*C	-0.039
A*D	7.274
A*E	104
B*C	0.0208
B*D	2.489
B*E	4.9
C*D	-0.254
C*E	17.1
D*E	89

Table A.3. Simplified ANOVA for Thermal Resistance

Source	Adj MS	F-Value	P-Value
Linear	1.09582	231.98	0.000
(A)Diameter	0.03808	8.06	0.006
(B)Pitch Ratio	0.04996	10.58	0.002
(C)HS Length	0.00028	0.06	0.809
(D)Fin Height	3.24378	686.69	0.000
(E)mass flow rate	2.20136	466.01	0.000
Square	0.07258	15.36	0.000
(A)*(A)	0.00004	0.01	0.923
(B)*(B)	0.01419	3.00	0.089
(C)*(C)	0.00143	0.30	0.585
(D)*(D)	0.09107	19.28	0.000
(E)*(E)	0.02568	5.44	0.024
2-Way Interaction	0.08826	18.68	0.000
(A)*(B)	0.18172	38.47	0.000
(A)*(C)	0.00039	0.08	0.774
(A)*(D)	0.55344	117.16	0.000
(A)*(E)	0.00210	0.44	0.508
(B)*(C)	0.00031	0.07	0.798
(B)*(D)	0.17995	38.09	0.000
(B)*(E)	0.00001	0.00	0.958
(C)*(D)	0.00750	1.59	0.213
(C)*(E)	0.00063	0.13	0.716
(D)*(E)	0.00069	0.15	0.704

Table A.4. Simplified ANOVA for Pressure Drop

Source	Adj MS	F-Value	P-Value
Linear	17.090	3379.85	0.000
(A)Diameter	3.1624	625.39	0.000
(B)Pitch Ratio	5.2633	1040.87	0.000
(C)HS Length	0.0037	0.74	0.394
(D)Fin Height	58.976	11663.0	0.000
(E)mass flow rate	17.167	3395.06	0.000
Square	0.1225	24.22	0.000
(A)*(A)	0.0020	0.40	0.529
(B)*(B)	0.0008	0.16	0.687
(C)*(C)	0.0132	2.61	0.112
(D)*(D)	0.2989	59.11	0.000
(E)*(E)	0.1655	32.74	0.000
2-Way Interaction	0.3611	71.42	0.000
(A)*(B)	0.2321	45.89	0.000
(A)*(C)	0.0040	0.79	0.377
(A)*(D)	1.8718	370.16	0.000
(A)*(E)	0.0049	0.96	0.330
(B)*(C)	0.0003	0.05	0.825
(B)*(D)	1.5168	299.95	0.000
(B)*(E)	0.0007	0.15	0.704
(C)*(D)	0.0033	0.66	0.421
(C)*(E)	0.0002	0.05	0.829
(D)*(E)	0.0371	7.33	0.009